

# THE NEAR- AND MID-INFRARED CONTINUUM EMISSION OF SEYFERT NUCLEI: CONSTRAINTS ON THE MODELS OF OBSCURING TORI

DARIO FADDA<sup>1,2,4</sup>, GIULIANO GIURICIN<sup>1,2</sup>, GIAN LUIGI GRANATO<sup>3</sup> AND DONATELLA VECCHIES<sup>1,2</sup>

<sup>1</sup>Dipartimento di Astronomia, Università degli Studi di Trieste,

<sup>2</sup>SISSA, via Beirut 4, 34013 – Trieste, Italy

<sup>3</sup> Osservatorio Astronomico di Padova, Vicolo dell'Osservatorio 5, 35122 – Padova, Italy

<sup>4</sup> Osservatorio Astronomico di Trieste, Via Tiepolo 11, 34131 –Trieste, Italy

E-mail: fadda@sissa.it; giuricin@sissa.it; granato@pdmida.pd.astro.it; dona@sissa.it

## ABSTRACT

For an extended sample of Seyfert galaxies we compile from the literature the infrared fluxes in the four IRAS bands, the ground-based small-beam ( $\sim 5\text{--}10''$ ) fluxes in the standard Q, N, M, L (or L') bands, and the nuclear (non-stellar) estimated fluxes in the JHK bands. We estimate nuclear fluxes in the L band by applying a correction for stellar light.

From the statistical study of the infrared colors and luminosities, we derive the typical SEDs of Seyfert 1 and 2 nuclei and the typical differences in luminosities between the two types of objects in the mid- and near-infrared spectral ranges. The analyses of colors and luminosities agree with the fact that in general Seyfert 2 nuclei become increasingly fainter with respect to Seyfert 1 as we go toward shorter infrared wavelengths. This behavior is consistent with growing anisotropy of a dusty torus emission towards shorter wavelengths, but the degree of anisotropy is low (the radiation appears to be substantially isotropic at  $\lambda \gtrsim 25 \mu\text{m}$ ). For Seyfert 2 galaxies having Compton-thin obscuring structures at hard X-ray energies, we find correlations between the absorbing hydrogen columns and some infrared colors and luminosities.

The observational data appear to severely challenge many models of dusty tori, which hardly account for the shapes of the SEDs and the degree of anisotropy observed in Seyfert galaxies. In particular, at variance with some earlier claims, very thick and compact tori are basically inconsistent with these observational constraints. The most successful models, though having problems in accounting for several details, can fit the major infrared observational data of both Seyfert 1 and Seyfert 2 nuclei with tori which extend up to several hundreds pc and have fairly low optical thickness.

*Subject headings:* galaxies: active – galaxies:nuclei – galaxies: Seyfert – infrared: galaxies

## 1 INTRODUCTION

Large amounts of observational data have been accumulated during the last decade supporting unified models of active galactic nuclei (AGNs), particularly of Seyfert galaxies. The canonical unified model of Seyfert galaxies claims that Seyfert 1 galaxies (S1s) contain the same central engines as Seyfert 2 galaxies (S2s), but have the broad-line region and the strong optical/UV/X-ray continuum of the central source concealed from our view by a disk or torus of dusty molecular clouds (see, e.g., the review by Antonucci, 1993). This obscuring structure would absorb a significant fraction of the optical/UV/X-ray luminosity and should therefore radiate this energy strongly in the infrared (IR). This would explain why Seyfert galaxies are strong IR emitters. They appear to be relatively brighter than non-Seyfert ones at near-infrared (NIR) and mid-infrared (MIR) wavelengths on the basis of the global spectral energy distributions (SEDs) and relevant central colors (e.g., Spinoglio et al., 1995; Glass & Moorwood, 1985; Giuricin et al., 1994).

Dust reprocessing of the primary emission is at present regarded as the most likely source of the bulk of the strong NIR and MIR emission of radio-quiet quasars and Seyfert galaxies. Observational evidence favoring models in which the IR emission predominantly or entirely comes from

heated dust is summarized by Barvainis (1992).

Geometric, energetic, and spectropolarimetric arguments indicate that the optical/UV continuum escapes anisotropically from the nuclei of at least some Seyfert objects. The presence of extended ionization cones which are seen in images of emission lines around several S2 galaxies (see, e.g., the review by Wilson, 1996) suggests that the ionizing radiation emitted from the nucleus is collimated. The observed ionizing photon deficit in S2s (Binette, Fosbury & Parker, 1993) indicates that the central ionized gas responds to a higher photon flux than that seen along our line of sight. Broad hydrogen emission lines, presumably transmitted through the torus, have been detected in the IR spectra of some S2 galaxies. (Blanco, Ward & Wright, 1990; Goodrich, Veilleux & Hill, 1994; Ruiz, Rieke & Schmidt, 1994). These kinds of arguments suggest the presence of an obscuring dusty torus in S2 objects (see, e.g., the review by Wilson (1992) for a discussion of these topics). The X-ray spectra of S2s exhibit absorptions larger than those of S1s, providing strong support for the presence of an obscuring structure (e. g., Nandra & Pounds, 1994; Smith & Done, 1996).

The first models of thermal dust emission for the origin of the IR emission of Seyfert galaxies and radio-quiet quasars simply involve optically thin dust configurations (e.g., Barvainis, 1987, 1990, Loska, Szczerba & Czerny,

1993), which imply too small an optical depth at optical/UV wavelengths ( $\tau \lesssim 3$ ), or configurations in idealized slab geometry (Laor & Draine, 1993). Phinney (1989; see also Sanders et al., 1989) modeled the IR continua of AGNs as thermal emission from a dusty warped disk which extends for a few kpc in the host galaxy; but its large radial extent would imply an unreasonably large mass, if the warped structure were not transparent enough at IR wavelengths.

In recent years radiative transfer calculations specific to the IR emission of thick, dusty axisymmetric torus-like structures have been carried out by Pier & Krolik (1992, 1993, hereafter PK), Granato & Danese (1994; hereafter GD), Efsthathiou & Rowan–Robinson (1995; hereafter ER). All these models concur that face-on systems (i.e., S1s within the unified scheme of Seyfert galaxies) should be, on average, stronger NIR and MIR emitters than edge-on systems (i.e., S2s) for a wide range of torus geometries and optical depths, whilst at long enough IR wavelengths the two types of objects should appear to be similar. However, the predicted IR emission and degree of IR anisotropy differ in many details.

As is expected in many models of optically thick tori, the observations indicate that Seyfert galaxies display a broad IR bump which peaks in the MIR. S2s exhibit steeper IR continua between NIR and far-infrared (FIR) wavelengths than S1s do (Edelson, Malkan & Rieke, 1987), although an accurate determination of the SEDs of the two types of objects is hampered at NIR wavelengths by appreciable starlight contributions, which are typically greater for S2s (Alonso-Herrero, Ward & Kotilainen). Moreover, some authors have claimed that S2s are characterized by lower mean N-band ( $\lambda \sim 10 \mu\text{m}$ ) luminosities than those of S1s (Heckman 1995; Maiolino et al., 1995). The last two facts can be interpreted as anisotropy resulting from the presence of an obscuring torus.

Furthermore, the observations show that the MIR spectra of S2s typically display strong silicate absorption bands (at  $\lambda \sim 10 \mu\text{m}$ ), whereas those of S1 are mostly featureless (Roche et al., 1991). The elusiveness of emission features in the MIR spectra of Seyfert galaxies represents a serious challenge to many models of tori.

Comparisons between IR observations and theoretical predictions have been presented in several above-mentioned papers for fairly small samples of Seyfert galaxies (see also Granato, Danese & Franceschini, 1997). But the IR SEDs predicted by torus models and, in particular, the level of IR anisotropy deserve to be better tested through an extensive statistical analysis of the IR properties of Seyfert galaxies. Their NIR and especially MIR continua, where the peak of the torus emission is expected to occur, are key spectral regions in which to probe the structure of the obscuring–reprocessing torus.

In this paper, in order to test models of IR torus emission, we analyze the MIR and NIR photometric data of a wide sample of Seyfert galaxies. Specifically, we compile from the literature IRAS fluxes (at  $\lambda \sim 12, \sim 25, \sim 60, \sim 100 \mu\text{m}$ ), ground-based small-aperture ( $\sim 5\text{--}10''$ ) pho-

tometric measurements in the standard Q ( $\lambda \sim 20 \mu\text{m}$ ), N ( $\lambda \sim 10 \mu\text{m}$ ), M ( $\lambda \sim 4.8 \mu\text{m}$ ), L ( $\lambda \sim 3.5 \mu\text{m}$ ) or L' ( $\lambda \sim 3.8 \mu\text{m}$ ) bands, and available non-stellar (nuclear) flux estimates in the J ( $\lambda \sim 1.25 \mu\text{m}$ ), H ( $\lambda \sim 1.6 \mu\text{m}$ ), K ( $\lambda \sim 2.2 \mu\text{m}$ ) bands.

In §2 we describe the data sample compiled from the literature. In §3 we analyze the MIR, NIR colors and luminosities of our Seyfert galaxies with the main purpose of establishing the relevant SEDs of S1 and S2 nuclei and the differences in their typical relevant luminosities. We also explore relations between these properties and some hard X-ray properties. We use survival analysis techniques (see, e. g., the review by Feigelson, 1992) in order to exploit the information contained in censored data (i.e., upper limits on fluxes). In practice we use the software package ASURV (Rev 1.2, La Valle, Isobe & Feigelson, 1992), in which the methods presented in Feigelson & Nelson (1985) and in Isobe, Feigelson & Nelson (1986) are implemented. Ensuing constraints on the models of IR torus emission are discussed in §4. Lastly, §5 summarizes our results and contains our conclusions.

## 2 THE DATA SAMPLE

We have considered a wide sample of Seyfert galaxies ( $\sim 700$  objects) having  $z < 0.1$ . Our sample essentially contains all known Seyfert galaxies having  $z < 0.05$  and many more distant objects. The objects have been taken from the lists of Dahari & De Robertis (1988), Whittle (1992), de Grijp et al. (1992), Nelson & Whittle (1995), and the catalogue of Véron–Cetty & Véron (1996). Like several wide samples of Seyfert galaxies considered in the literature, our sample is likely to be biased towards objects which are bright at optical and infrared wavelengths.

The Seyfert type classification is primarily based on the spectroscopic study of the CfA Seyfert sample by Osterbrok & Martel (1993) and on the first four above-mentioned papers. The Seyfert types are grouped into the three types S1 (types 1 and 1.2), S1.5 (types 1.5) and S2 (types 1.8, 1.9, 2). The distances D of the nearby galaxies which are included in Tully’s (1988) NBG catalog are taken directly from the values tabulated therein. The distances of non-cluster NBG galaxies have been essentially estimated on the basis of velocities, an assumed  $H_0 = 75 \text{ km s}^{-1} \text{ Mpc}^{-1}$  and a Virgocentric retardation model in which the author assumed that the Milky Way is retarded by  $300 \text{ km s}^{-1}$  from the universal Hubble flow by the mass of the Virgo cluster. Non-NBG galaxies are given redshift distances D with the same value of  $H_0$ .

We have collected the IRAS fluxes (at  $\lambda \sim 12, \sim 25, \sim 60, \sim 100 \mu\text{m}$ ) of our Seyfert objects preferentially from specific reference sources which report co-added survey data (e.g., Rush, Malkan & Spinoglio (1993), Sanders et al. (1995), de Grijp et al. (1992), Edelson et al. (1987), Sanders et al. (1989), Mazzarella, Bothun & Boroson (1991), Knapp, Bies & van Gorkom (1990), Knapp et al. (1989), Soifer et al. (1989), Bothun et al. (1989), Hill, Becklin & Wynn–Williams (1988), Rice et al (1988), Helou

et al. (1988), Salzer & MacAlpine (1988), Golombek, Miley & Neugebauer (1988)), and from the IRAS Faint Source Catalog (see Moshir et al., 1992), in order of preference. We have found IRAS data (detections or  $3\sigma$  upper limits) at  $\lambda \sim 12, \sim 25, \sim 60, \sim 100 \mu\text{m}$  for 535, 538, 540, 539 objects, respectively.

We have considered the recent estimates of the non-stellar (nuclear) near-infrared (NIR) J, H, K fluxes. We have taken relevant NIR data primarily from the observational studies by Kotilainen et al. (1992a,b), who observed a hard X-ray-selected sample of Seyfert galaxies (nearly all S1), Danese et al. (1992) and Zitelli et al. (1993), who observed Markarian S1 and S1.5 objects, Kotilainen & Prieto (1995), who studied NGC 5252, and Alonso-Herrero, Ward & Kotilainen (1996), who investigated S2 objects. From NIR imaging observations (often complemented by NIR aperture photometry) these authors obtained accurate estimates of the contribution to the total NIR emission arising from the nuclear source alone by decomposing the surface brightness profiles into a combination of a nuclear source, a bulge component and a disc component. For NGC 5548 and Mk 509 we have adopted the averages of the NIR nuclear fluxes derived by Kotilainen et al. (1992a) and Danese et al. (1992). The resulting data sample contains nuclear J, H, K fluxes for 73 (41 S1, 12 S1.5, 21 S2), 73 (41 S1, 12 S1.5, 21 S2), and 79 (46 S1, 12 S1.5, 21 S2) objects respectively. Moreover, we have taken some L-band nuclear magnitudes estimated by Alonso-Herrero et al. (1996) through model parameters obtained in the K band, L aperture photometry and standard K-L colors of normal galaxies.

We have gathered other (less accurate) K-band nuclear data from McLeod & Rieke (1995) and from Heisler, De Robertis & Nadeau (1996) for 24 and 15 objects respectively. In their own K-band imaging observations of CfA Seyfert objects the former authors have approximated the nuclear source as a stellar point spread function scaled to the central intensity of the light profile; this approach tends to overestimate the nuclear source contribution. Heisler et al. (1996) have reported NIR images of a sample of IRAS galaxies whose SED peaks in the IRAS  $\lambda \sim 60 \mu\text{m}$  band and have derived the nuclear K-band magnitudes of their Seyfert objects from the observed  $H\alpha$  luminosities simply by assuming Case B recombination and a power-law SED with a spectral index  $n = -1$  ( $F_\nu \propto \nu^n$ ) in the optical and NIR bands.

In addition, a few JHKL nuclear data have been taken from Ward et al. (1987) for NGC 4051 and from McAlary & Rieke (1988) for Mk 6, Mk 1040, NGC 2992, NGC 6814, I 4329A (for which mean values have been adopted). Ward et al. (1987) have fitted the light profile obtained from R-band CCD images with three components (point source, disk, and bulge) and have then extrapolated the derived nuclear contribution into the infrared assuming normal stellar colors. McAlary & Rieke (1988) employed a Hubble-law growth curve, modified by a color-morphological type-aperture relation, to deconvolve multi-aperture optical and NIR photometry of Seyfert ob-

jects into stellar and non-stellar nuclear emissions.

Moreover, we have gathered together from the literature all published ground-based, small-aperture ( $\sim 5''$ – $10''$ ) photometric measures in the Q, N, M, L or L' standard broad bands. L' band measures are considered only for objects which lack small-beam L photometry. The consultation of the "Catalog of Infrared Observations" by Gezari et al. (1993) has been of valuable aid in compiling infrared photometric data from the literature. In the case of multiple entries for an object, we have adopted the mean values of the fluxes published in a reference source. Non-detections are reported as  $3\sigma$  upper limits on fluxes; in case of no detection we have chosen the most stringent upper limits on fluxes.

In general we have preferred the smallest beam size measures, in order to minimize the inclusion of starlight in MIR fluxes. In any case, we have preferentially selected the sets of multi-wavelength observations published by the same authors (e.g., the sets of measures by Rieke (1978), McAlary et al. (1983), Lawrence et al. (1985), Rudy & Rodríguez-Espinosa (1985), Edelson et al. (1987), Ward et al. (1987), Neugebauer et al. (1987), Hill et al. (1988), in order to minimize the effects of data inhomogeneity and infrared variability (if any) in the definition of the spectral energy distributions (SEDs) of our objects. Long time-scale variations of JHKL band fluxes have been frequently observed in Seyfert galaxies (e.g., Kotilainen et al., 1992b; Glass, 1992), whereas no sure evidence of variability at longer infrared wavelengths has been noted in Seyfert galaxies and radio-quiet quasars (e.g., Edelson & Malkan, 1987; Neugebauer et al., 1989). Thus, we have paid particular attention to selecting L (or L') fluxes and JHK nuclear fluxes measured at the same epoch (if available). For this reason we have selected the JHKL nuclear fluxes of NGC 2992 and I 4329 A as given by McAlary & Rieke (1988) (instead of Kotilainen et al.'s (1982a) values), because they are based on small-beam ( $4.6''$ ) JHKL photometric observations which are simultaneous (McAlary et al., 1983).

Most of the QNML(L') photometric data have been taken from the papers mentioned above and from Stein & Weedmann (1976), McAlary, McLaren & Crabtree (1979), Rudy, Levan & Rodríguez-Espinosa (1982), Glass & Moorwood (1985), Boisson & Durret (1986), Carico et al. (1988), Sanders et al. (1989), Kotilainen et al. (1992), Zitelli et al. (1993), Wynn-Williams & Becklin (1993), Vader et al. (1993), Elvis et al. (1994), Maiolino et al. (1995), and Alonso-Herrero et al. (1996). We have found Q, N, M, L (or L') data (detections or upper limits) for 45 (20 S1, 5 S1.5, 20 S2), 173 (65 S1, 17 S1.5, 91 S2), 36 (14 S1, 7 S1.5, 15 S2), and 202 (79 S1, 21 S1.5, 102 S2) objects, respectively.

If magnitudes are given in the literature, they have been generally converted to fluxes by means of Wilson et al.'s (1972) zero-magnitude calibration. In view of the fairly large photometric errors (i.e.,  $\sim 10\%$ ,  $\sim 10\%$ ,  $\sim 20\%$ ,  $\sim 20\%$ ,  $\sim 25\%$  for the L, L', M, N, Q fluxes), no corrections have

been applied for interstellar extinction and redshift.

Finally, we have considered the measures of [OIII] $\lambda$ 5007A narrow emission line flux available in the literature for 364 objects (105 S1, 35 S1.5, 224 S2), as compiled mostly by Nelson & Whittle (1995), Whittle (1992), Dahari & De Robertis (1988), de Grijp et al. (1992), Mulchaey, Wilson & Tsvetanov (1996a).

The starlight contribution dramatically decreases as we go from the JHK bands to longer wavelengths (see, e.g., the JHKL nuclear fluxes estimated by Ward et al. (1987) and McAlary & Rieke (1988)). Also the image sizes of luminous infrared galaxies are smaller at  $\lambda \sim 3.4 \mu\text{m}$  than at shorter IR wavelengths (e.g., Zhou, Wynn-Williams & Becklin, 1993). The small-beam fluxes in the QNM bands of our Seyfert objects can be taken essentially as nuclear fluxes.

On the other hand, the stellar contribution is still appreciable within small-beam L fluxes; within 3 arcsec it ranges between fractions of  $\sim 10\%$  to  $\sim 50\%$  (with a mean of  $\sim 30\%$ ) for S2s, which, however, show a greater starlight contribution in the JHKL bands than S1s (Alonso-Herrero et al., 1996). Therefore, we have corrected the published L (or L') fluxes by subtracting an estimated value for starlight. This was done by assuming that the J-band flux, which has been taken in the same aperture and preferentially by the same authors as the L (or L') measurements, consists entirely of starlight which has  $J-L=+1.3$ ; this is the normal color for an old stellar population coming from observations of elliptical galaxies and bulge-dominated regions of spiral galaxies (e.g., Willner et al., 1984). Any superposing thermal emission from central hot dust would enhance the L-band flux much more than the J-band flux so that the resulting overcorrection in L would be negligible.

Since a few galaxies lack J-band photometry, the resulting sample of galaxies with L-band nuclear fluxes or relevant upper limits comprises 200 objects (78 S1, 21 S2, 101 S2). We have checked that our rough method would give L nuclear magnitudes similar to those less crudely derived by Alonso-Herrero et al. (1996) for 11 galaxies (in this case we directly took their values). In a few cases our L-band correction is slightly greater than the measured L-band fluxes. For these galaxies, which have probably very little or no L-band flux associated with an active nucleus, we have adopted an upper limit of  $F_{L_n} < 1 \text{ mJy}$ .

The large-beam IRAS MIR fluxes at  $\sim 12$  and  $\sim 25 \mu\text{m}$  certainly include emission coming from the host galaxies. However, their good correlations with the K nuclear emission and the N emission suggest that the bulk of IRAS MIR emission of Seyfert galaxies comes from the nuclear region, at variance with the IRAS FIR emission (at  $\lambda \sim 60$  and  $\sim 100 \mu\text{m}$ ) which mostly originates from the host galaxies (see, e.g., Danese et al., 1992; Giuricin, Mardirossian & Mezzetti, 1995). This is also directly revealed by the high-resolution IR images of the central regions of nearby Seyfert galaxies, since these observations clarify the relative role of AGN and star formation in producing the IR emission (see e.g. the review by Telesco

(1988) and the MIR maps of NGC 1068 (Telesco & Decher, 1988), NGC 1808, NGC 1365, and NGC 5506 (Telesco, Dressel & Wolstencroft, 1993), NGC 7469 (Miles, Houck & Hayward, 1994)). Therefore, in this paper we mainly deal with the IRAS MIR fluxes. We use the IRAS FIR fluxes only for some comparisons.

Throughout this paper the fluxes measured in the IRAS  $\lambda \sim 25$  and  $\sim 12 \mu\text{m}$ , Q, N, M bands and the non-stellar (nuclear) estimated fluxes in the L, K, H, J bands are respectively denoted by  $F_{25}$ ,  $F_{12}$ ,  $F_Q$ ,  $F_N$ ,  $F_M$ ,  $F_{L_n}$ ,  $F_{K_n}$ ,  $F_{H_n}$ ,  $F_{J_n}$ . The corresponding monochromatic luminosities  $L_\nu$  (expressed in W/Hz) and the luminosity  $L_{[\text{OIII}]}$  (in erg/s) of the [OIII] $\lambda$ 5007

A emission line follow from the adopted distances (with  $H_0=75 \text{ km s}^{-1} \text{ Mpc}^{-1}$ ). We have always used L'-band measures in place of L-band measures, if the latter are not available. We have verified that S1 objects alone give results (color and luminosity distributions) similar to those of S1+S1.5 objects. Therefore, in the following sections the latter objects will be simply denoted as S1s.

### 3 ANALYSIS AND RESULTS

#### 3.1 The IR colors

In order to establish the behavior of the IR continuum at MIR and NIR wavelengths, we have evaluated the following colors (decimal logarithm of flux ratios)  $\log(F_{25}/F_{12})$ ,  $\log(F_Q/F_N)$ ,  $\log(F_N/F_M)$ ,  $\log(F_M/F_{L_n})$ ,  $\log(F_N/F_{L_n})$ ,  $\log(F_N/F_{K_n})$ ,  $\log(F_{L_n}/F_{K_n})$ ,  $\log(F_{K_n}/F_{H_n})$ ,  $\log(F_{H_n}/F_{J_n})$  separately for S1+S1.5 and S2 galaxies. We have evaluated the nine above-mentioned colors (or relevant lower or upper limits) for all objects detected in the two relevant bands and also for the objects having upper limits on  $F_{12}$ ,  $F_Q$ ,  $F_M$ ,  $F_N$ ,  $F_N$ , for the first six colors, respectively. The very few objects having upper limits on the other term of a given ratio or those which have upper limits on both terms are excluded. There are only detections for the case of the last three colors.

We have employed the Kaplan-Meier product limit estimator (which is part of the ASURV package) in order to calculate the median, mean and distribution functions of the colors of the two groups of Seyfert galaxies. Redistributing upper limits (if any) uniformly along all the intervals of lower detected values, the Kaplan-Meier estimator provides an efficient, non-parametric reconstruction of information lost by censoring in the case of randomly censored data sets. We compare the distribution functions of colors for the two classes of Seyfert galaxies by testing the "null" hypothesis that the two independent random samples are randomly drawn from the same parent population. In the case of uncensored data, this is accomplished by using the Kolmogorov-Smirnov test (see e.g. Hoel, 1971). In the general case of censoring we use two versions of Gehan's test (one for permutation variance and the other with hypergeometric variance), the logrank, the Peto-Peto, and Peto-Prentice tests.

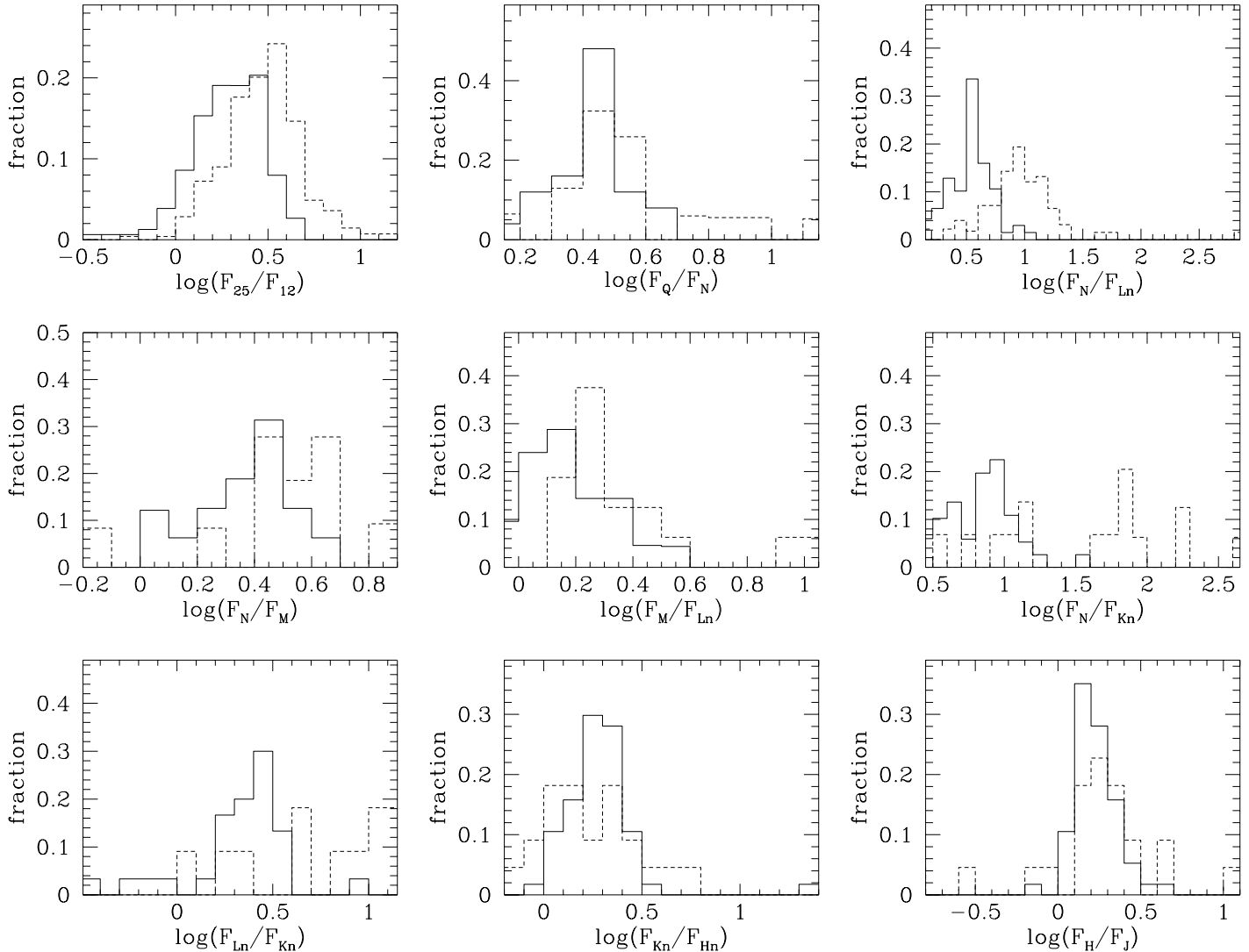


FIG. 1.— The histograms show the color distributions for S1 (solid lines) and S2 nuclei (dashed lines).

These two-sample tests give the probability  $p$  that the two data samples would be drawn from one parent population. The statistical significance of the difference between the color distributions of the two classes of galaxies is at the  $100(1-p)\%$  level. The two-sample tests differ in how the censored points are weighted and consequently have different sensitivities and efficiencies with different distributions and censoring patterns.

### 3.1.1 The color distributions

Table 1 gives the numerical outcomes, namely the total number of objects  $N$ , the number  $N_{ul}$  of relevant upper limits, the median and mean values (with associated  $1\sigma$  errors), and the corresponding median spectral index  $n$  ( $F_\nu \propto \nu^{-n}$ ) for the distributions of the above-mentioned nine colors. Fig. 1 shows the Kaplan-Meier distributions of the colors for S1 and S2 objects.

In general S2s have redder  $\log(F_{25}/F_{12})$ ,  $\log(F_Q/F_N)$ ,  $\log(F_N/F_M)$ ,  $\log(F_M/F_{L_n})$ ,  $\log(F_N/F_{L_n})$ ,  $\log(F_N/F_{K_n})$ ,  $\log(F_{L_n}/F_{K_n})$  colors (i.e., steeper SEDs) than S1s. Table 2 contains the mean and median values of the probability  $p$  that the colors of S1 and S2 objects would be drawn from the same parent population. One can see that the statistical significance of the color differences between the two groups of galaxies is high in several cases and marginal in the cases of  $\log(F_Q/F_N)$  and  $\log(F_N/F_M)$ . On the other hand, the two groups of Seyfert objects do not differ appreciably in the  $\log(F_{K_n}/F_{H_n})$  and  $\log(F_{H_n}/F_{J_n})$  distributions.

We have attempted to investigate the possible effects of circumnuclear star formation on IR colors. Although it is difficult to come up with consistent quantitative indicators of this phenomenon, it does not seem to occur very frequently in nearby Seyfert objects (e.g., Pogge, 1989).

TABLE 1

THE IR COLORS

Color	Sample	$N$	$N_{ul}$	Median	Mean	$n$
(1)	(2)	(3)	(4)	(5)	(6)	(7)
hline $\log(F_{25}/F_{12})$	S1	157	26	$0.31^{+0.0}_{-0.04}$	$0.28 \pm 0.02$	1.0
	S2	276	77	$0.49^{+0.01}_{-0.01}$	$0.47 \pm 0.02$	1.5
$\log(F_Q/F_N)$	S1	25	0	$0.42^{+0.04}_{-0.01}$	$0.42 \pm 0.02$	1.4
	S2	19	3	$0.47^{+0.11}_{-0.03}$	$0.55 \pm 0.06$	1.6
$\log(F_N/F_{Ln})$	S1	67	8	$0.55^{+0.01}_{-0.03}$	$0.54 \pm 0.02$	1.2
	S2	66	9	$0.93^{+0.03}_{-0.03}$	$0.94 \pm 0.05$	2.0
$\log(F_N/F_M)$	S1	18	2	$0.45^{+0.03}_{-0.09}$	$0.37 \pm 0.04$	1.4
	S2	12	1	$0.57^{+0.06}_{-0.15}$	$0.50 \pm 0.07$	1.8
$\log(F_M/F_{Ln})$	S1	23	2	$0.18^{+0.02}_{-0.05}$	$0.18 \pm 0.03$	1.3
	S2	16	0	$0.27^{+0.13}_{-0.06}$	$0.39 \pm 0.07$	2.0
$\log(F_N/F_{Kn})$	S1	38	4	$0.87^{+0.03}_{-0.04}$	$0.85 \pm 0.04$	1.3
	S2	16	1	$1.69^{+0.18}_{-0.53}$	$1.56 \pm 0.16$	2.6
$\log(F_{Ln}/F_{Kn})$	S1	30	0	$0.36^{+0.04}_{-0.02}$	$0.32 \pm 0.05$	1.8
	S2	11	0	$0.75^{+0.27}_{-0.10}$	$0.74 \pm 0.11$	3.7
$\log(F_{Kn}/F_{Hn})$	S1	57	0	$0.27^{+0.02}_{-0.01}$	$0.28 \pm 0.03$	2.0
	S2	22	0	$0.19^{+0.15}_{-0.02}$	$0.25 \pm 0.05$	1.4
$\log(F_{Hn}/F_{Jn})$	S1	57	0	$0.20^{+0.02}_{-0.0}$	$0.22 \pm 0.02$	1.9
	S2	22	0	$0.23^{+0.08}_{-0.02}$	$0.22 \pm 0.08$	2.1

In any case, the galaxies which are known to have clear signs of intense circumnuclear star formation (e.g., NGC 1068, NGC 1365, NGC 1808, NGC 3982, NGC 4388, NGC 4945, NGC 5427, NGC 5728, NGC 5953, NGC 6221, NGC 7469, NGC 7582, NGC 7592, I 4553, Circinus galaxy), as is evidenced mostly by spectroscopic investigations of nuclear spectra or emission line imaging surveys (e.g. Véron-Cetty & Véron, 1986; Pogge, 1989, Evans et al., 1996), do not appear to have colors significantly different from the norm.

TABLE 2

THE P-VALUES FOR THE IR COLOR DISTRIBUTIONS

Color	Mean $p$	Median $p$
(1)	(2)	(3)
$\log(F_{25}/F_{12})$	< 0.0001	< 0.0001
$\log(F_Q/F_N)$	0.138	0.087
$\log(F_N/F_{Ln})$	< 0.0001	< 0.0001
$\log(F_N/F_M)$	0.059	0.065
$\log(F_M/F_{Ln})$	0.007	0.009
$\log(F_N/F_{Kn})$	0.002	0.0001
$\log(F_{Ln}/F_{Kn})$	0.0009	0.0009
$\log(F_{Kn}/F_{Hn})$	0.21	0.21
$\log(F_{Hn}/F_{Jn})$	0.63	0.63

The color distributions are in general Gaussian and unimodal, with some exceptions mentioned below. We have adopted the probability  $P_W$  associated with the W-test (Shapiro & Wilk, 1965) in order to estimate the Gaussianity of the color distributions for uncensored data.

We have computed the dispersions of the color distributions for the uncensored data only. We have compared these observational dispersions  $\sigma_{obs}$  with the values  $\sigma_{cal}$

which are expected from reasonable observational uncertainties on the fluxes, using the first order approximation  $\sigma(\log x) \simeq \log(e)\sigma(x)/x$ . We have adopted the following percentage errors: 10% on  $F_{25}$ , 15% on  $F_{12}$ , 25% on  $F_Q$ , 20% on  $F_N$ , 20% on  $F_M$ , 15% on  $F_{Ln}$ , 30% on  $F_{Kn}$ ,  $F_{Hn}$ ,  $F_{Jn}$ .

As shown by Table 3, the expected values ( $\sigma_{cal}$ ) are almost always smaller than the observed ones ( $\sigma_{obs}$ ). This indicates the presence of appreciable intrinsic dispersion in the IR colors. The observed dispersions for S2s are typically greater than those for S1s even at the longest IR wavelengths, where uncertainties in the fluxes are similar for the two types of objects.

Some comments on the individual color distributions follow.

### 3.1.2 The mid-IR colors

Let us discuss the MIR colors  $\log(F_{25}/F_{12})$  and  $\log(F_Q/F_N)$ . The distribution of  $\log(F_{25}/F_{12})$  for S1s presents a tail at low values which makes its shape a little different from a Gaussian one (the W-test applied to the uncensored data gives a probability  $P_W=0.026$  that the distribution does not deviate from Gaussianity). For S1s, our  $\log(F_{25}/F_{12})$ -distribution is shifted to somewhat lower values than previous distributions based on much smaller data samples, whilst it essentially confirms previous typical results for S2s (Giuricin et al., 1995; Maiolino et al., 1995).

The  $\log(F_Q/F_N)$ -distribution, as yet unexplored in the literature, has mean and median values similar to those of the  $\log(F_{25}/F_{12})$ -distribution for S2s. On the other hand, S1s lead to a  $\log(F_Q/F_N)$ -distribution which is shifted to somewhat greater values than the  $\log(F_{25}/F_{12})$  one.

TABLE 3

THE DISPERSIONS OF THE IR COLOR DISTRIBUTIONS

Color	$\sigma_{obs}$ S1	$\sigma_{obs}$ S2	$\sigma_{cal}$
(1)	(2)	(3)	(4)
$\log(F_{25}/F_{12})$	0.19	0.21	0.08
$\log(F_Q/F_N)$	0.12	0.25	0.14
$\log(F_N/F_{Ln})$	0.18	0.40	0.11
$\log(F_N/F_M)$	0.17	0.25	0.12
$\log(F_M/F_{Ln})$	0.16	0.27	0.11
$\log(F_N/F_{Kn})$	0.23	0.75	0.16
$\log(F_{Ln}/F_{Kn})$	0.27	0.37	0.15
$\log(F_{Kn}/F_{Hn})$	0.19	0.25	0.18
$\log(F_{Hn}/F_{Jn})$	0.13	0.39	0.18

The evaluation of the  $\log(F_{25}/F_{12})$  distributions for the 25 S1s and 17 S2 objects with available  $\log(F_Q/F_N)$  confirms the presence of some systematic differences for S1s, since their distribution leads to a median value of 0.31 and a mean value of 0.32. Consistently, a steepening of the MIR SED of S1 objects towards shorter wavelengths is suggested by Roche et al.'s (1991) MIR spectrophotometric observations. These authors noted that the slopes

of the  $\lambda \sim 8\text{--}13 \mu\text{m}$  spectra they obtained on ground-based telescopes with small beams ( $\sim 5''$ ) were steeper than the IRAS 12–25  $\mu\text{m}$  slopes for galaxies with featureless MIR spectra (mostly S1s).

### 3.1.3 The mid-to-near IR colors.

The seeming bimodality of the  $\log(F_N/F_M)$ -histogram is not statistically significant. The  $\log(F_M/F_{L_n})$  distribution for S2s presents a tail at high values, which makes it significantly non-Gaussian. ( $P_W=0.002$ ). The  $\log(F_N/F_M)$  and  $\log(F_M/F_{L_n})$  distributions give results which are substantially consistent with those relative to the  $\log(F_N/F_{L_n})$  distributions, since they imply median (mean) values of  $\log(F_N/F_{L_n})$  equal to 0.63 (0.55) and 0.84 (0.89) for S1s and S2 objects, respectively. The  $\log(F_N/F_{L_n})$ -distribution for S2s is significantly more peaked than a Gaussian distribution ( $P_W < 0.0001$ ). In the following we shall adopt the  $\log(F_N/F_{L_n})$ -distribution in order to define the SED between the relevant wavelengths, because the statistics are better and there is no significant indication of a change (at  $\lambda \sim 4.8 \mu\text{m}$ ) in the SED slopes of the two types of objects. We point out that neglecting a correction for starlight in the L-band, one obtains an appreciable overestimate of this color also for small-beam observations of nearby objects. For instance, the  $\log(F_N/F_L)$ -distributions of 67 S1 and 66 S2 objects lead to median (mean) values of 0.44 (0.42) and 0.74 (0.72), respectively. Compared to the results of the corresponding  $\log(F_N/F_{L_n})$ -distributions, this implies a median L-band starlight contribution of 28% and 55% for the two groups of objects, respectively. Correction for starlight is generally neglected in the relevant literature, except in Pier & Krolik (1993). Encouragingly, relying on the small data sample (15 S1s and 6 S2s) considered by these authors, we obtain similar medians of  $\log(F_N/F_{L_n})$  (i. e.,  $\sim 0.6$  and 0.9, respectively).

The two fluxes used to compute the quantities  $\log(F_{25}/F_{12})$ ,  $\log(F_Q/F_N)$ ,  $\log(F_N/F_M)$ ,  $\log(F_M/F_{L_n})$ ,  $\log(F_N/F_{L_n})$  come from the same reference sources in many cases. This limits the effect of data inhomogeneity on these five colors. This problem may be more serious for the sample of  $\log(F_N/F_{K_n})$ , in which the two fluxes generally come from different reference sources and refer to measurements carried out in different epochs. We have obtained a  $\log(F_N/F_{K_n})$ -distribution characterized by median (mean) values of 0.87 (0.87) for 51 S1s (with 6 upper limits on  $F_N$ ) and 1.06 (1.30) for 38 S2s (with 4 upper limits on  $F_N$ ). But we have preferred to rely finally on a subsample of bona fide  $\log(F_N/F_{K_n})$  colors, by considering only objects with  $F_{K_n}$  data taken from the accurate decomposition analyses by Kotilainen et al. (1992a, b), Danese et al. (1992), Zitelli et al. (1993), Kotilainen & Prieto (1995), and Alonso-Herrero et al. (1996). Table 1 and Fig. 1 present our results for this selected subsample, which, compared to the above-mentioned wider sample, substantially confirms the median and mean values of the  $\log(F_N/F_{K_n})$  distribution for S1s, but leads to redder colors for S2s. The addition of a few objects having  $F_{K_n}$

estimates taken from Ward et al. (1987) and McAlary & Rieke (1988) yields a  $\log(F_N/F_{K_n})$  distribution which is similar to that of the selected subsample. On the other hand, the inclusion of  $F_{K_n}$  fluxes taken from McLeod & Rieke (1995) and Heisler et al. (1996) tends to shift the  $\log(F_N/F_{K_n})$  distribution of S2s to appreciably smaller and larger values, respectively, and gives rise to an even broader and more irregular (i.e., non-Gaussian) color distribution than the broad one of the selected subsample. The large proportion of  $F_{K_n}$  data taken from McLeod & Rieke (1995) in the wide sample accounts for the above-mentioned difference in the median colors of S2s.

### 3.1.4 The near-IR colors

The sample of  $\log(F_{L_n}/F_{K_n})$  colors leads to a distribution characterized by median (mean) values of 0.34 (0.34) for 66 S1s (with no censoring) and 0.65 (0.75) for 44 S2s (with one upper limit on  $F_{L_n}$ ). But this sample suffers from the same problems of inhomogeneity which affect the  $\log(F_N/F_{K_n})$  colors. Therefore, also in this case we have preferred to rely on a selected subsample of bona fide  $\log(F_{L_n}/F_{K_n})$  colors, by considering only objects with both good  $F_{K_n}$  data (defined as above) and with  $F_{L_n}$  fluxes derived from L band data measured by the same authors in similar epochs; the latter requirement is intended to avoid the possible effects of nuclear variability. Table 1 and Fig. 1 refer to this selected subsample, which, however, substantially confirms the typical values given by the wider sample for both S1s and S2s. These two distributions were found to be not significantly different from those of the selected subsamples through the application of the usual two-sample tests, although the selected subset of S2s seems to lead to a narrower spread of values and that of S1s shows a tail at low values ( $P_W=0.007$ ). Incidentally, a somewhat larger subsample which contains only objects with good  $F_{K_n}$  data (as above), but with no restrictions on the reference sources for the  $F_{L_n}$  data, again essentially confirms the typical values listed in Table 1.

The quantities  $\log(F_N/F_{L_n})$ - and  $\log(F_{L_n}/F_{K_n})$  yield results which are in substantial agreement with those given by the  $\log(F_N/F_{K_n})$ -distribution, since for this quantity they imply median values of 0.91 (for S1s) and 1.68 (for S2s). The SEDs of both types of objects considerably steepen beyond the L-band (i.e., at shorter wavelengths). In the following we shall use the colors  $\log(F_N/F_{L_n})$ - and  $\log(F_{L_n}/F_{K_n})$  to establish the SEDs between relevant wavelengths.

As regards the quantities  $\log(F_{K_n}/F_{H_n})$  and  $\log(F_{H_n}/F_{J_n})$ , S2s show distributions which are broader than those of S1s, but they are centered at similar values and have no significant bimodality. We have verified that the distributions of these two quantities do not change appreciably, if we restrict these two data samples to objects with  $F_{K_n}$  data taken from the accurate decomposition analyses by Kotilainen et al. (1992a, b), Danese et al. (1992), Zitelli et al. (1993), Kotilainen & Prieto (1995), and Alonso-Herrero et al. (1996).

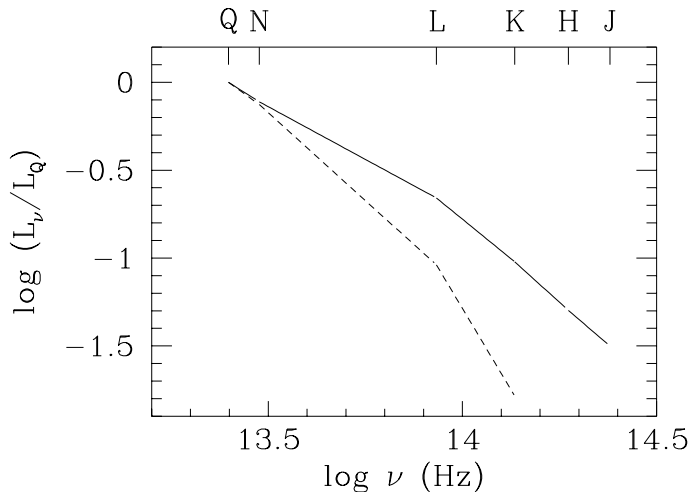


FIG. 2.— This figure shows the median SEDs of S1 (solid lines) and S2 nuclei (dashed lines). The two SEDs are arbitrarily normalized so that they match at long wavelengths ( $\lambda = 20 \mu\text{m}$ , Q-band).

The absence of any statistical difference between S1s and S2s in these two colors is clearly unexpected. It is likely to reflect very large uncertainties associated with the delicate estimates of nuclear fluxes in the H and J bands for S2s, where the starlight contribution is even greater than in the K band (see, e. g., Alonso–Herrero et al., 1996; Kotilainen et al., 1992a). Therefore, in the following we will adopt take into consideration only the results relative to S1s, disregarding those relative to S2s.

Fig. 2 illustrates the adopted median SEDs of S1 and S2 nuclei as they result from the colors discussed above. The two SEDs are arbitrarily normalized so that they match at long wavelengths ( $\lambda=20 \mu\text{m}$ ). Since S2s always have steeper SEDs than the former objects, the degree of difference between the luminosities  $L_\nu$  of the two groups of objects increases towards shorter wavelengths.

### 3.1.5 Correlations involving colors

We have investigated the correlations between colors by computing the two non-parametric rank correlation coefficients, Spearman’s  $r_s$  and Kendall’s  $r_k$  (see, e.g., Kendall & Stuart, 1977), in cases of uncensored quantities. In testing the significance of the correlations between the variables  $x$  and  $y$  containing censored data, we have relied on the Cox proportional hazard model, the generalized Kendall rank correlation statistics, and the generalized Spearman rank–order correlation coefficient. The first method allows censored data for only one variable, whereas the last two methods also allow simultaneous censoring in both variables.

As expected, the quantity  $\log(F_{25}/F_{12})$  appears to correlate significantly with  $\log(F_Q/F_N)$  for both S1s and S2s (at the median, one-tailed significant levels of 96.5% and 99.2%, respectively).

TABLE 4

THE IR LUMINOSITY DISTRIBUTIONS

Variable	Sample	$N$	$N_{ul}$	Median	Mean
(1)	(2)	(3)	(4)	(5)	(6)
$\log L_{25}$	S1	203	45	$23.66^{+0.03}_{-0.08}$	$23.57 \pm 0.07$
	S2	335	60	$23.57^{+0.05}_{-0.03}$	$23.53 \pm 0.04$
$\log L_{12}$	S1	203	69	$23.32^{+0.09}_{-0.09}$	$23.24 \pm 0.08$
	S2	332	131	$23.03^{+0.06}_{-0.05}$	$23.01 \pm 0.05$
$\log L_Q$	S1	25	0	$23.78^{+0.23}_{-0.12}$	$23.73 \pm 0.13$
	S2	20	3	$22.99^{+0.23}_{-0.16}$	$23.13 \pm 0.17$
$\log L_N$	S1	82	15	$23.29^{+0.17}_{-0.07}$	$22.94 \pm 0.15$
	S2	91	14	$22.58^{+0.16}_{-0.08}$	$22.58 \pm 0.08$
$\log L_M$	S1	21	0	$22.91^{+0.23}_{-0.02}$	$22.83 \pm 0.16$
	S2	15	0	$22.47^{+0.19}_{-0.52}$	$22.44 \pm 0.26$
$\log L_{Ln}$	S1	99	2	$22.71^{+0.09}_{-0.08}$	$22.65 \pm 0.07$
	S2	101	8	$21.79^{+0.10}_{-0.06}$	$21.84 \pm 0.08$
$\log L_{Kn}$	S1	58	0	$22.39^{+0.19}_{-0.05}$	$22.41 \pm 0.07$
	S2	21	0	$21.13^{+0.21}_{-0.26}$	$21.09 \pm 0.17$

In general we have detected no other significant correlations, with the exception of a  $\log(F_{25}/F_{12}) - \log(F_N/F_{Ln})$  correlation for S1 galaxies ( $N=68$ , 99.0% significance level), which holds also for uncensored data.

We have verified that no color correlates with the galaxy distances (for both S1s and S2s). Subsamples of nearby objects give similar color distributions.

Moreover, we have searched for correlations between colors and some indicators of the MIR luminosities such as  $L_N$ ,  $L_{12}$ ,  $L_{25}$ , because MIR emission, being an approximate constant fraction of the bolometric flux of Seyfert nuclei, is believed to provide the best indication of the nuclear bolometric luminosity (Spinoglio & Malkan, 1989; Spinoglio et al., 1995). In general, we have detected no correlations, except for the color  $\log(F_{25}/F_{12})$ , which shows a slight tendency to be somewhat greater in S1 and S2 objects of greater MIR luminosities. This behavior is dissimilar from that shown by  $\log(F_{60}/F_{25})$  and  $\log(F_{100}/F_{60})$ , which tend to decrease with increasing MIR luminosity in Seyfert galaxies. The latter behavior could be ascribed to a decreasing relative contribution of the cool emission from galaxy disks in high–luminosity AGNs (Giuricin et al., 1995).

### 3.2 The IR luminosities

We are interested in establishing the differences between the typical luminosities of S1s and S2s in different bands, because appreciable differences are predicted by torus models (especially for very optically thick configurations and/or at the shortest IR wavelengths). For the sake of comparison with samples published in the literature, in Table 4 we list the total number of objects  $N$ , the number of upper limits  $N_{ul}$ , the mean and median values of  $L_\nu$  together with associated  $1\sigma$  errors, for the two groups of objects and different spectral bands.

Table 4 reveals that S1s tend to be more luminous than S2s at the shortest IR wavelengths, but this may be par-

tially due to observational selection effects which favor the observation of luminous objects at great distances (S1s are typically more distant than S2s). In order to remove this distance selection effect in the comparison of groups of objects lying at different typical distances, for each spectral band we have considered the logarithmic relation

$$\log L_\nu = 17.078 + \log(F_{\nu,min}) + 2\log D \quad (1)$$

which yields the minimum value of  $\log L$  (with  $L_\nu$  in W/Hz) corresponding to the minimum uncensored or censored value of  $F_\nu$  ( $F_{\nu,min}$ ) for an object at distance  $D$  (in Mpc). Obviously, upper limits and the detections of the faintest objects cluster near this relation in the  $\log L_\nu - \log D$  diagram. In the case of  $L_{K_n}$ , we have taken the subset of objects with  $F_{K_n}$  data taken from the accurate decomposition analyses by Kotilainen et al. (1992a, b), Danese et al. (1992), Zitelli et al. (1993), Kotilainen & Prieto (1995), and Alonso-Herrero et al. (1996).

We have used relation (1) to evaluate the *observed* minus *calculated* value of  $\log L_\nu$ , i. e.  $\Delta(\log L_\nu)$ , for each object. In this manner we have obtained  $\Delta(\log L_\nu)$ -distributions that are free from distance selection effects. Table 5 lists the total number of objects  $N$ , the number of upper limits  $N_{ul}$ , the mean and median values of  $\Delta(\log L_\nu)$  (together with associated  $1\sigma$  errors), for the two groups of objects and different spectral bands. Fig. 3 displays the  $\Delta(\log L_\nu)$ -distributions for the most interesting cases. There is no significant evidence of bimodality in the  $\Delta(\log L_\nu)$ -distributions. The statistical significance of the

difference between the distributions of the two groups of objects has been evaluated through the application of the above-mentioned five two-sample tests. In several cases the non-random character of the censoring pattern tends to give asymmetrical distributions. However, since two-sample tests seek only to compare two samples, they do not require that the censoring patterns of the two samples be random.

Table 5 and Fig. 3 reveal that S2 galaxies have, on average, greater  $L_{25}$  luminosities than S1s by a median factor of  $\sim 1.5$  (at a significance level corresponding to  $p < 0.0001$ ). The  $L_Q$  distributions give consistent results, although the difference is never statistically significant, because of the relatively low number of objects. As we go towards shorter wavelengths the difference between the typical luminosities of the two classes first disappears (see, e.g.,  $L_{12}$  and  $L_N$ ) and then reappears in the opposite sense (see  $L_{L_n}$  and  $L_{K_n}$ ). As a matter of fact, the  $L_{L_n}$  luminosities of S2s are significantly fainter than those of S1s by a factor 1.8 (with a median  $p=0.0004$ ). In other words, as we go from  $L_{25}$  to  $L_{L_n}$ , the ratio of the S2 luminosities over S1 luminosities typically decreases by a factor of  $\sim 2.7$ . The  $L_{K_n}$  luminosities of S2s are significantly fainter than those of S1s by a factor  $\sim 3.5$  (with a median  $p < 0.0001$ ); the total sample of  $L_{K_n}$  data gives  $\sim 3.7$ . Hence, in going from  $L_{25}$  to  $L_{K_n}$ , S2s become typically fainter than S1s by a factor  $\sim 5.2$  ( $\sim 5.5$  for the total sample). We have verified that subsamples of nearby objects always give similar results for all spectral bands.

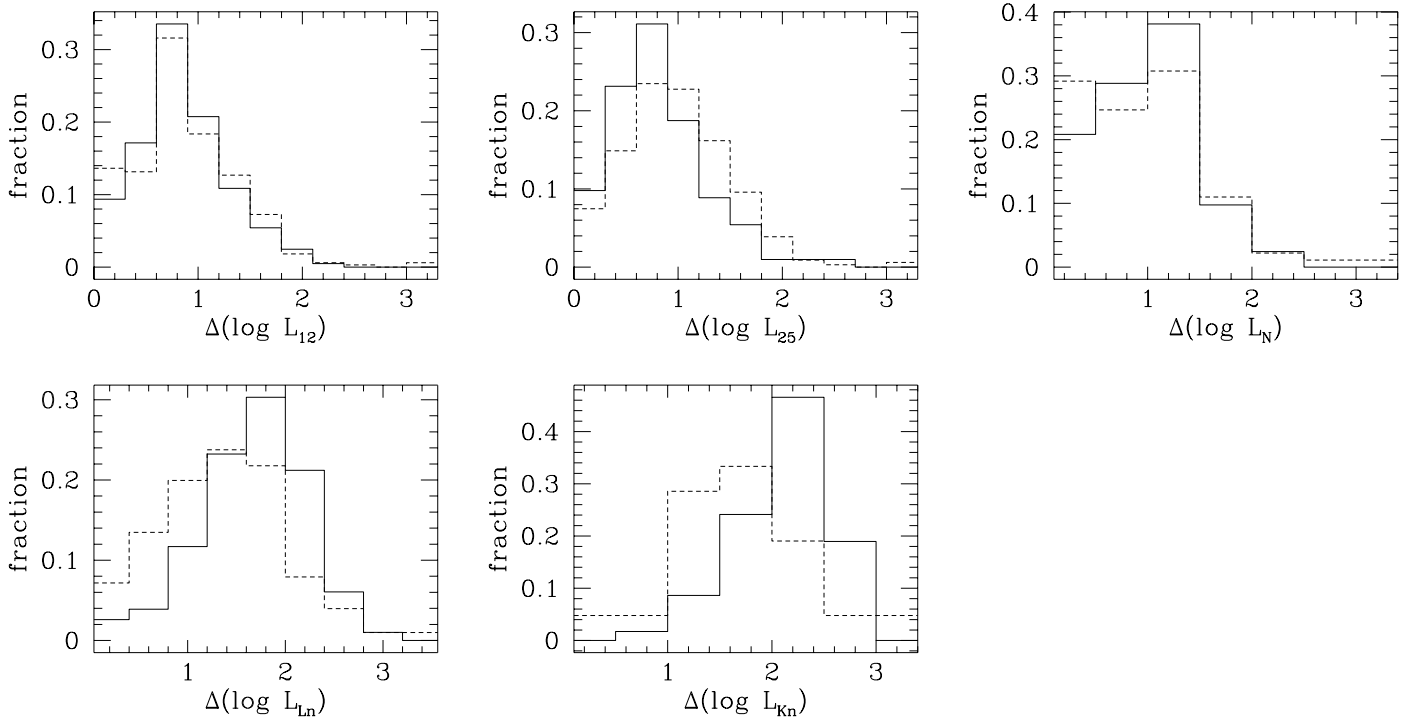


FIG. 3.— The histograms show the distributions of  $\Delta(\log L_\nu)$  relative to different photometric bands, for S1 (solid lines) and S2s (dashed lines).  $\Delta(\log L_\nu)$  is the *observed* minus *calculated* value of the logarithm of the monochromatic luminosity.

TABLE 5

THE  $\Delta(\log L_\nu)$  LUMINOSITY DISTRIBUTIONS

Variable	Sample	$N$	$N_{ul}$	Median	Mean
(1)	(2)	(3)	(4)	(5)	(6)
$\Delta \log L_{25}$	S1	203	45	$0.78^{+0.04}_{-0.04}$	$0.81 \pm 0.04$
	S2	335	60	$0.95^{+0.03}_{-0.03}$	$1.01 \pm 0.03$
$\Delta \log L_{12}$	S1	203	69	$0.82^{+0.03}_{-0.03}$	$0.86 \pm 0.04$
	S2	332	131	$0.82^{+0.03}_{-0.03}$	$0.87 \pm 0.04$
$\Delta \log L_Q$	S1	25	0	$0.50^{+0.21}_{-0.05}$	$0.61 \pm 0.07$
	S2	20	3	$0.77^{+0.21}_{-0.09}$	$0.85 \pm 0.14$
$\Delta \log L_N$	S1	82	15	$0.98^{+0.13}_{-0.09}$	$0.97 \pm 0.06$
	S2	91	14	$0.90^{+0.11}_{-0.07}$	$0.96 \pm 0.07$
$\Delta \log L_M$	S1	21	0	$0.58^{+0.02}_{-0.03}$	$0.60 \pm 0.08$
	S2	15	0	$0.73^{+0.10}_{-0.15}$	$0.82 \pm 0.15$
$\Delta \log L_{Ln}$	S1	99	2	$1.66^{+0.07}_{-0.18}$	$1.66 \pm 0.06$
	S2	101	8	$1.40^{+0.08}_{-0.10}$	$1.37 \pm 0.07$
$\Delta \log L_{Kn}$	S1	58	0	$2.17^{+0.09}_{-0.10}$	$2.10 \pm 0.06$
	S2	21	0	$1.62^{+0.11}_{-0.08}$	$1.64 \pm 0.16$

Interestingly, the increasing dimming of S2s towards shorter wavelengths (with respect to S1s) agrees with the differences between the SEDs of S1s and S2s and with the expectations of models of obscuring tori emitting anisotropic radiation at short enough wavelengths. But it is a little surprising that S2s appear to be typically brighter than S1s at  $\lambda \sim 25 \mu\text{m}$ , because in the framework of torus models S2s are expected to have similar or smaller luminosities. By the way, in the same manner we have found that S2s are typically brighter than S1s also at IRAS  $\lambda \sim 60$  and  $\sim 100 \mu\text{m}$  bands by similar median factors, i.e.  $\sim 1.5$  and  $\sim 1.7$ , respectively.

We have deemed it useful to check this point by considering some subsamples, namely the UV excess-selected Markarian objects, the IRAS 12  $\mu\text{m}$  flux-limited Seyfert galaxies listed by Rush et al. (1993), and the IRAS sample by de Grijp et al. (1992), who selected objects with relatively warm 25  $\mu\text{m}$  to 60  $\mu\text{m}$  colors. Only the first and second subsamples confirm the dissimilarity between the  $\Delta(\log L_\nu)$ -distributions of S1s and S2s in the three above-mentioned IRAS bands. This dissimilarity turns out to be fairly strong in the first subsample (where it amounts to a factor of  $\sim 1.6$  for  $\Delta(\log L_{25})$ ), weak in the second subsample (where the corresponding factor is  $\sim 1.3$ ), whilst it disappears in the third one. Hence, there is no sure evidence of an intrinsic difference between the two classes of objects. Our results may simply reflect a selection effect in several current samples, in the sense that S2s undergoing active star formation are more likely to be detected at short IR wavelengths and especially at optical wavelengths than objects not undergoing star formation. Thus star formation may seem more common in galaxy disks hosting S2 nuclei than in those containing S1s, as recently stressed by Maiolino et al. (1995), who examined the extended MIR emission of Seyfert galaxies by comparing the  $\lambda \sim 10 \mu\text{m}$  ground-based observations with the IRAS  $\lambda \sim 12 \mu\text{m}$  fluxes. The aforementioned selection effect may also explain why circumnuclear star formation seems to be

a little more common in S2s than in S1s, as suggested by the emission line imaging surveys of nearby Seyfert galaxies (e.g., Pogge (1989) and Evans et al. (1996)).

We have provided a further check on this point by comparing the distributions of the IR luminosities normalized to a quantity which is powered by the active nucleus and is presumed to be isotropic, i.e. free of viewing angle effects, like optical emission lines produced in the NLR, hard X-ray emission and central radio continuum emission (e.g., Mulchaey et al., 1994). We have chosen to use the luminosity of the [OIII] $\lambda 5007$  A emission line, because it gives the widest data sample, although this quantity can be affected by NLR dust absorption (e.g., Dahari & De Robertis, 1988a) and torus obscuration, as was suggested in the case of radio galaxies (Jackson & Brown (1990), Hes, Barthel & Fosbury (1993), Laing et al. (1994)). Although extended line emission may be missed in small-aperture measurements, these measures are less dependent than radio fluxes on the size of the observed region (the central radio emission of Seyfert galaxies has been recently discussed by Giuricin, Fadda & Mezzetti, 1996).

S1s and S2s have  $\log(L_{[\text{OIII}]})$ -distributions characterized by mean (median) values of 41.15 (41.22) for  $N=140$  objects and 40.90 (41.02) for  $N=224$  objects (with  $L_{[\text{OIII}]}$  in erg/s), together with  $\Delta \log(L_{[\text{OIII}]})$ -distributions characterized by corresponding values of 1.55 (1.57) and 1.56 (1.52). The two  $\Delta \log(L_{[\text{OIII}]})$ -distributions do not differ, which is in line with the common view that the two types of Seyfert galaxies have the same [OIII] properties (e.g., Dahari & De Robertis, 1988a; Keel et al., 1994; Mulchaey et al., 1994; Mulchaey, Wilson & Tsvetanov, 1996b). Comparing the distributions of the quantities  $\log(L_{12}/L_{[\text{OIII}]})$ ,  $\log(L_Q/L_{[\text{OIII}]})$ ,  $\log(L_{25}/L_{[\text{OIII}]})$ ,  $\log(L_{60}/L_{[\text{OIII}]})$ ,  $\log(L_{100}/L_{[\text{OIII}]})$  by means of the usual two-sample tests we have again found that S2s have brighter normalized luminosities than S1s, in the last five bands, by similar median factors (i.e.  $\sim 1.5$ ,  $\sim 1.4$ ,  $\sim 1.8$ ,  $\sim 1.7$ , respectively), whereas they do not differ from S1s at  $\lambda \sim 12 \mu\text{m}$ . The analysis of the quantities  $\log(L_N/L_{[\text{OIII}]})$ ,  $\log(L_{Ln}/L_{[\text{OIII}]})$ ,  $\log(L_{Kn}/L_{[\text{OIII}]})$  shows that S2s have fainter normalized luminosities than S1s by median factors of  $\sim 1.5$ ,  $\sim 2.4$ ,  $\sim 5.9$ , respectively. Again we have verified that subsamples of nearby objects give similar results.

Incidentally, within extended data samples (though smaller than ours) examined in the literature, de Grijp et al. (1992) and Keel et al. (1994) found similar FIR luminosities for the S1 and S2 objects of their IR-selected sample, whereas Dahari & De Robertis (1988) and Mulchaey et al. (1994) noted enhanced normalized IRAS luminosities (at least in one of the above-mentioned three bands) for the S2s of their samples which are dominated by Markarian objects. All these results are consistent with what we found for the overall sample and subsamples based on different selection criteria.

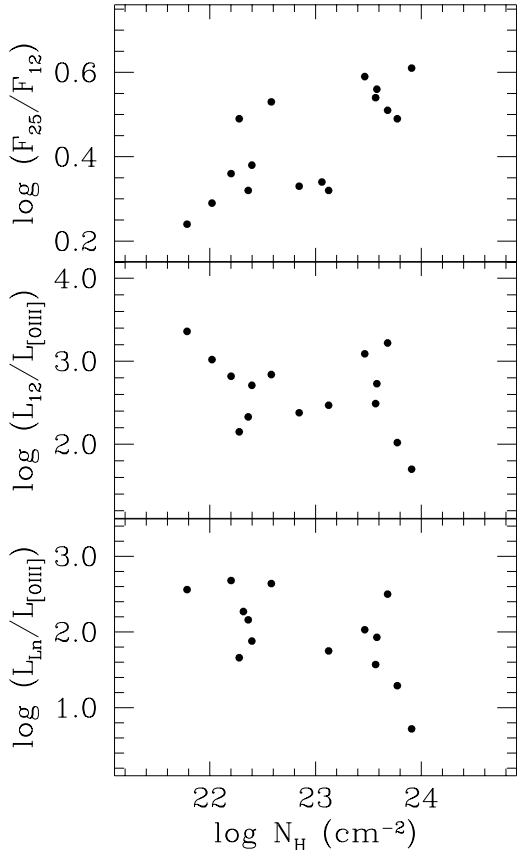


FIG. 4.— The plots show the correlations between infrared quantities and the absorbing hydrogen columns  $N_H$  (expressed in  $cm^{-2}$ ). The infrared luminosities are integrated luminosities evaluated as  $\nu L_\nu$ .

In any case, our results clearly favor models in which obscuring structures are essentially isotropic emitters already at  $\lambda \sim 25$   $\mu m$ . It is encouraging that the degree of the increasing faintness of S2s towards shorter wavelengths (with respect to S1s) – as derived from a comparison of the luminosities – turns out to be in fairly good, quantitative agreement with what we expect from the differences between the SEDs of the two groups of objects. S2s are found to be fainter than S1s by a typical factor of  $\sim 1.5$  at  $\lambda \sim 12$   $\mu m$ , of  $\sim 2.7$  at  $\lambda \sim 3.5$   $\mu m$ , of  $\sim 5$ – $7$  at  $\lambda \sim 2.2$   $\mu m$ . (Specifically in the last case, values of  $\sim 5.2$  and  $\sim 6.6$  are derived from the differences in the luminosities and in the SEDs, respectively.) The analysis of the IR luminosities normalized to  $L_{[OIII]}$  – an analysis which we regard as less reliable than the previous ones – gives similar results at long IR wavelengths and gives a somewhat more pronounced dimming of S2s at short IR wavelengths.

Within the framework of torus models these numbers establish the degree of anisotropy of the IR emission. Notably, we find a lower degree of anisotropy than that predicted by many torus models (see next section) and claimed by Heckman (1995). For instance, examining the distributions of  $\log(L_N/L_R)$ , where  $L_R$  is the central radio luminosity at the frequency of 1.4 GHz, Heckman (1995) argued that S1s are typically brighter than S2s by a factor

TABLE 6

CORRELATIONS BETWEEN  $N_H$  AND IR PROPERTIES

Variables (1)	N (2)	$r_S$ (3)	$r_K$ (4)
$N_H - \log(F_{25}/F_{12})$	16	0.71 (99.90%)	0.52 (99.76%)
$N_H - \log(L_{12}/L_{[OIII]})$	15	-0.36 (90.44%)	-0.22 (87.25%)
$N_H - \log(L_{Ln}/L_{[OIII]})$	14	-0.58 (98.56%)	-0.45 (98.76%)

of  $\sim 4$  (a result which is plagued by the large inhomogeneity of the radio fluxes); the distributions of  $\log(L_N/L_{[OIII]})$  yielded a lower factor of  $\sim 2$ , which is less inconsistent with ours. Our results are closer to those of Maiolino et al. (1995) and Giuricin et al. (1995), who derived a milder anisotropy from the direct comparisons of the  $L_N$  luminosities.

### 3.3 Relation between the IR properties and X-ray absorption

As is expected within the framework of torus models, the NIR and MIR emissions of Seyfert nuclei appear to be related to their hard X-ray emission (see Danese et al. (1992), Kotilainen et al. (1992b) and Giuricin et al. (1995), Barcons et al. (1995), respectively). Furthermore, Goodrich et al. (1994) noted that the S2 galaxies in which broad  $Pa\beta\lambda 1.2818\mu m$  emission lines have been detected are also the objects which generally have the lowest values of the X-ray absorbing hydrogen columns  $N_H$  derived from the hard X-ray spectra. Recently, Granato et al. (1997) found some evidence that the X-ray column depths of S2 galaxies show a negative correlation with their N-band emissions, at least for objects which have a so low Compton depth ( $N_H \lesssim 10^{24} cm^{-2}$ ) that the hard X-rays can be seen directly through the torus.

Our wide sample of IR data allows us to investigate further this point. To this end we have assembled the  $N_H$ -values (mean values in the case of multiple entries) as derived by Smith & Done (1996) (for power-law fits to GINGA data), Iwasawa (1996), Warwick et al. (1993) for 17 Compton-thin S2 objects. Their  $N_H$ -distribution ranges over  $6 \cdot 10^{21} \leq N_H \leq 10^{23}$  (with  $N_H$  in units of  $cm^{-2}$ ), with a median value of  $N_H = 7 \cdot 10^{22}$ , which is considerably greater than the median value  $N_H \sim 10^{21}$  of S1 objects (Nandra & Pounds, 1994), even though the S2 sample is biased towards low values of  $N_H$ .

We examined the correlations between  $N_H$  and the IR colors discussed in §3.1 and those between  $N_H$  and the IR luminosities (normalized to the  $L_{[OIII]}$  luminosities) discussed in §3.2. As regards the colors, only  $\log(F_{25}/F_{12})$  displays a significant (positive) correlation with  $N_H$ ; the other colors show no correlations (but the number of objects is smaller). As regards the luminosities,  $\log(L_{12}/L_{[OIII]})$  shows a marginal anti-correlation with  $N_H$  (but  $\log(L_{25}/L_{[OIII]})$  does not for the same objects) and  $\log(L_{Ln}/L_{[OIII]})$  displays a strong anti-correlation; the lack of correlation for the other colors may simply be

due to the smaller number of objects. Fig. 4 illustrates the three above-mentioned significant correlations and Table 6 presents the relevant results. In this table we list the two correlation coefficients, Spearman's  $r_s$  and Kendall's  $r_k$ , together with the associated (one-tailed) percent significance levels (in these cases we have only detected objects).

If we added in also the data for a few S2 galaxies which are likely to have Compton-thick ( $N_H > 10^{24} \text{cm}^{-2}$ ) obscuring structures (i. e., NGC 1068, NGC 4945, NGC 6552, and the Circinus galaxy; see, e.g., Matt et al., 1996, and references cited therein) so that their hard X-ray emission is presumably due to a scattered nuclear component, all the correlations would vanish. This enlarged, less biased, sample of S2 objects has a median value of  $N_H \sim 2.9 \cdot 10^{23} \text{cm}^{-2}$ .

In summary, our study provides further support for the contention that the IR emitting torus is related to the X-ray absorbing structure, but only for Compton-thin structures.

#### 4 COMPARISON WITH THEORETICAL MODELS

The IR colors and the degree of anisotropy of the IR emission derived in the previous section can be compared with the relevant predictions of a wide series of torus models (PK, GD, ER) characterized by different geometries, opacities and viewing angles. We have computed the theoretical colors and anisotropies by filtering the predicted IR SEDs through the typical overall spectral responses (including filter transmission, detector response and atmospheric transmission), which were taken from Bessell & Brett (1988) for the JHKL photometry, from Campins, Rieke & Lebofsky (1995) for the NQ photometry, from Beichman et al. (1988) for IRAS photometry.

##### 4.1 Models of compact cylinders

PK modeled the torus simply as a geometrically thick, annular ring of uniform density dust which surrounds a central point source of radiation. PR proposed cylindrical configurations characterized by small extension (radial sizes  $\lesssim$  a few pc) and very large optical thickness, in order to fit the general shape of the IR SED of Seyfert galaxies (in particular that of the S2 galaxy NGC 1068) and the appearance of the  $\sim 10 \mu\text{m}$  silicate feature, which is seen in absorption in many S2 objects, whereas it is undetected in many S1 galaxies. Specifically, they preferred models with radial and vertical Thomson depths  $\tau_r = \tau_z = 1$  (corresponding to a visual extinction  $A_V \sim 750$  mag and a hydrogen column density  $N_H = 1.5 \cdot 10^{24} \text{cm}^{-2}$  for standard dust and dust-to-gas ratio), an inner radius-to-height ratio  $a/h \sim 0.3$ , and  $T_{\text{eff}} \sim 500\text{-}1000$  K (where  $T_{\text{eff}}$  is the effective temperature of the illuminating radiation on the inner wall of the torus). Basically, models with greater values of  $a/h$  or  $T_{\text{eff}}$  would shift the peak of the thermal bump to too short wavelengths and would lead to too warm IR colors, whereas models of low optical thickness ( $\tau_r = 0.1$  and/or  $\tau_z = 0.1$ ) would predict an (unobserved) prominent  $10 \mu\text{m}$  emission feature for face-on viewing angles.

Examining the predicted colors for face-on views (viewing angle  $i = 0^\circ$ ), we have noticed that published SEDs (for  $T_{\text{eff}} \sim 1000\text{-}2000$  K) are in general characterized by too warm (small) IR colors, with SEDs which peak at shorter wavelengths than observed. Only models with low values of  $T_{\text{eff}}$  ( $T_{\text{eff}} \sim 500$  K) and  $a/h$  ( $a/h \sim 0.1$ ) can reasonably fit the MIR colors (i.e.  $\log(F_{25}/F_{12})$  and  $\log(F_Q/F_N)$ ) of S1 objects, for the wide range of values of Thomson optical depths ( $\tau \sim 0.1\text{-}10$ ) explored by PK. But at shorter IR wavelengths those models imply a too steep IR SED, even for the choice of  $\tau$ -values which minimizes this problem (i. e.,  $\tau_z = \tau_r = 1$ ); the relevant colors would require models with greater values of  $a/h$  and  $T_{\text{eff}}$  ( $a/h \sim 0.3\text{-}1$ ,  $T_{\text{eff}} \sim 1000$  K). Similar problems hold for explaining both the long and short wavelength sides of the SEDs of S2s at the same time.

Recognizing a problem which is emphasized by our wide data sample, PK noted that the  $\log(F_N/F_{L_n})$  colors predicted by their preferred models were appreciably greater than the observed colors of a small sample of 15 S1 galaxies. In order to make the observed mid-to-near IR slope of these galaxies and PG quasars fit better with a broader IR bump, PR introduced a black body emission component ascribed to a small amount of hot ( $T \sim 1300$  K) dust which lies inside the inner edge of the torus and is hidden by its main body from edge-on views.

But the preferred optically thick tori, with  $\tau_z = \tau_r = 1$ ,  $a/h = 0.3$ ,  $T_{\text{eff}} \sim 500 - 1000$  K, entail an unreasonably large degree of anisotropy in the IR emission. For instance, they predict a ratio between the luminosities received by a polar ( $i = 0^\circ$ ) and equatorial ( $i = 90^\circ$ ) observer  $L_\nu(p)/L_\nu(e)$  equal to  $\sim 4\text{-}7$ ,  $\sim 10\text{-}20$ ,  $\sim 300\text{-}1500$  at  $\lambda \sim 25$ ,  $\mu\text{m}$ ,  $\sim 12 \mu\text{m}$ ,  $\sim 3.5 \mu\text{m}$ , respectively. For  $\cos i = 0.25$  in place of  $\cos i = 0$ , the corresponding ratios decrease respectively to  $\sim 2.5\text{-}3.0$ ,  $\sim 3\text{-}5$ ,  $\sim 7\text{-}10$ , which are still large values. Only tori of low opacity, which however do not fit other characteristics, would predict a mild enough degree of anisotropy; for instance, tori with  $\tau_z = \tau_r = 0.1$ ,  $a/h = 0.3$ ,  $T_{\text{eff}} = 1000$  K imply  $L_\nu(p)/L_\nu(e)$  equal to  $\sim 1.7$  and  $\sim 2.5$  at  $\lambda \sim 25 \mu\text{m}$  and  $\sim 12 \mu\text{m}$ .

##### 4.2 Models of tapered disks

In later models (GD, ER) inhomogeneous configurations with different outer shapes and density gradients were explored. ER discussed three different types of extended models, i. e. flared discs, anisotropic spheres, and tapered discs. They soon realized that flared discs suffer the main drawback of predicting very prominent  $10 \mu\text{m}$  emission features for face-on views. We have found that the two published models give too small colors for face-on views. For edge-on views, opaque models with equatorial optical depth  $\tau_{uv} = 200$  (where  $\tau_{uv} = \tau_{\lambda=1000\text{A}}$ ) reproduce colors better than configurations with relatively low opacity ( $\tau_{uv} = 40$ ), except for  $\log(F_N/F_{L_n})$ , which still remains too low, but they predict too large an anisotropy of the IR emission (for standard dust and dust-to-gas ratio  $A_V \sim 0.24 \tau_{uv}$ ). The authors noted that very optically thick and compact flared disks would reduce the strength

of the emission feature, but they would also produce too narrow an IR continuum.

Anisotropic spheres yield SEDs which show a more gradual transition from an edge-on to a face-on view than flared disks do. But face-on views still display strong  $10\ \mu\text{m}$  emission features and SEDs that are too flat in the MIR interval, whereas edge-on views, though predicting fairly realistic colors for opaque configurations ( $\tau_{uv} = 200$ ), with the exception again of  $\log(F_N/F_{Ln})$  which remains too low, give too large an anisotropy.

The authors devised tapered discs (discs whose height increases with distance from the central source but tapers off to a constant height in their outer part) mainly to suppress the  $10\ \mu\text{m}$  emission silicate features from face-on views, without imposing an excessive equatorial depth (which would entail an unreasonably narrow IR continuum) or without resorting to lower silicate efficiencies (as proposed by Laor & Draine, 1993) or silicate depletion by shocks (as proposed by GD). The tapered disk models assume the following main parameters: the opening angle of the disk  $\Theta_1$ , the ratio of inner to outer radii  $r_1/r_2$ , the ratio of the maximum half-thickness of the disc to the outer radius  $h/r_2$ , the equatorial optical depth  $\tau_{uv}$ , and the dust density distribution in radius.

The authors asserted that configurations with large opening angles ( $\Theta_1 \sim 60^\circ$ ) of the disk are unrealistic because they tend to show  $10\ \mu\text{m}$  absorption features from all viewing angles, whereas configurations with small opening angles ( $\Theta_1 \sim 30^\circ$ ) show implausible emission features for face-on views. Therefore, the authors deemed tapered disks with intermediate opening angles to be realistic and published the SEDs of four models with  $\Theta_1 = 45^\circ$ , among which they preferred the one which predicts an almost featureless MIR continuum together with a broad IR SED for face-on views. The preferred model is characterized by the following parameters:  $\Theta_1 = 45^\circ$ ,  $\tau_{uv} = 1500$ ,  $r^{-1}$  density distribution,  $r_1/r_2 = 0.01$ ,  $h/r_2 = 0.3$ .

We have found that none of the published models of tapered discs satisfactorily reproduce the observed small degree of anisotropy and the observed IR SEDs for face-on or edge-on views. In particular, the above-mentioned preferred model exhibits colors too large at longer IR wavelengths and too small at shorter IR wavelengths for edge-on views, together with too large colors at shorter IR wavelengths for face-on views. Besides, the model implies a large anisotropy corresponding to  $L_\nu(p)/L_\nu(e)$  equal to  $\sim 10$  and  $\gtrsim 50$  at  $\lambda \sim 25\ \mu\text{m}$  and  $\sim 12\ \mu\text{m}$ . For a viewing angle of  $i = 60^\circ$  the anisotropy, which remains large, decreases to  $\sim 2.5$  and  $\sim 7$  at  $\lambda \sim 25\ \mu\text{m}$  and  $\sim 12\ \mu\text{m}$ , respectively.

In conclusion, models of tapered disks, though having the virtue of solving problems related to the appearance of the  $10\ \mu\text{m}$  feature, do not seem to easily reproduce the typical shape of the NIR and MIR SEDs of Seyfert nuclei and the observed anisotropy.

Inspecting in detail NGC 1068, Efstathiou, Hough & Young (1996) realized that tapered disk models alone were unable to describe satisfactorily the IR SED of this object.

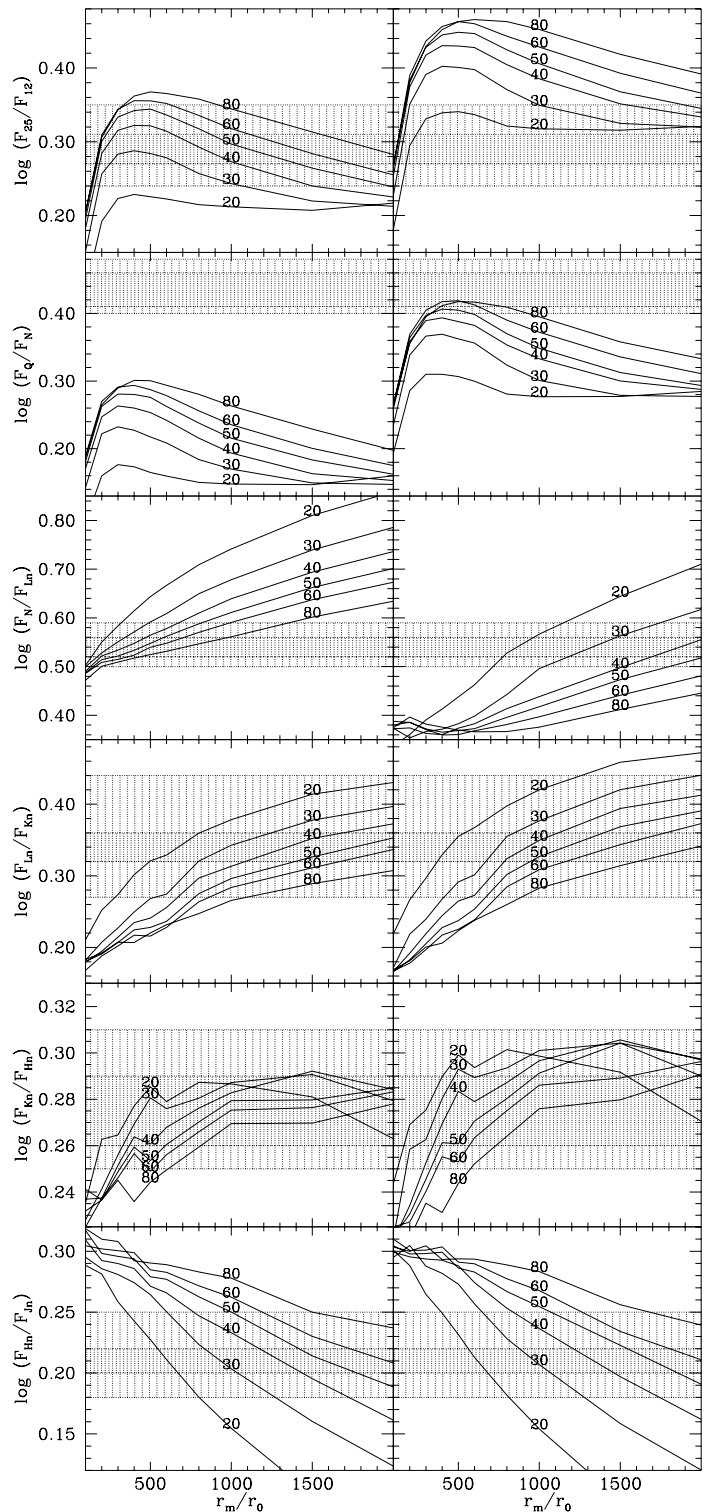


FIG. 5.— The plots show the colors predicted by torus models as a function of the outer-to-inner radius  $r_m/r_0$ , for values the equatorial optical thickness  $\tau_e$  ranging from 20 to 80, in case of a face-on viewing angle. The two hatched regions indicate the  $1 - \sigma$  and  $2 - \sigma$  error bars associated with the observed median. The left and right columns refer respectively to models with a standard silicate abundance and with a depression of silicates in the innermost regions.

Therefore, they supplemented the emission from the torus with an NIR component which was attributed to optically thin dust distributed in the ionization cone. In this way they obtained a more realistic SED, although the detailed fit of the  $10\ \mu\text{m}$  feature and of the extension of the NIR and MIR emissions are still difficult problems. We note that their composite model still implies a largely different SED for objects which are seen face-on and edge-on.

### 4.3 Models of flared disks

GD proposed flared disk configurations characterized by fairly large radial extension (from tens to hundreds pc), moderate optical thickness, an almost homogeneous density distribution, i.e. tori with equatorial optical depth  $\tau_e = \tau_{\lambda 3000\text{\AA}} \sim 10 - 100$  (for standard dust and dust-to-gas ratio  $A_V \sim 0.61 \cdot \tau_e$  mag. and  $N_H \sim 1.2 \cdot 10^{21} \tau_e \text{cm}^{-2}$ ), density distribution  $\rho \propto r^{-\beta}$  with  $\beta < 0.5$ , outer-to-inner radius ratio  $r_m/r_0 \sim 300 - 1500$  (where  $r_0 = 0.5 (L/10^{46} \text{erg/s})^{1/2}$  pc is set by the condition of sublimation of all dust species). In this way GD were able to reproduce the average shape of the IR SEDs of a sample of 16 optically-selected S1 objects, without resorting to additional IR emission components. In order to suppress the occurrence of the  $10\ \mu\text{m}$  silicate emission in these models for face-on views, GD proposed that shocks induced by radiation pressure depress the abundance of silicate grains in the innermost regions of tori (at  $r < \text{few} \cdot 10r_0$ ).

Recently, from several arguments, which include the  $\log F_N/F_{Ln}$  colors of a few nearby S2 galaxies and an upper limit on anisotropy in the MIR emission, Granato et al. (1997) argued in favor of moderately thick tori (with line-of-sight extinction  $A_V \lesssim 80$  mag) rather than of very thick configurations. Moreover, these authors fitted the IR SED of NGC 1068 with a line-of-sight extinction  $A_V \sim 50 - 100$  mag and with slightly less extended tori (with  $r_m/r_0 \sim 100 - 200$ ) than those proposed for S1s. If this were a general property of S2 galaxies, it would be a serious problem for the unified model of Seyfert galaxies. Clearly, this point deserves a statistical investigation such as the one we are carrying out in this paper.

Tori of moderate optical thickness such as those proposed by GD certainly promise to be successful models for explaining our observational results, which lead to a quite low degree of IR emission anisotropy. Thus, we have decided to undertake a detailed comparison between a wide series of GD torus models and observational data, in order to assess to what extent these models are compatible with our (partially new) results, which could provide more stringent constraints on torus properties. Using the GD code, we have computed the IR SEDs of many torus models for which we have always assumed a uniform density distribution ( $\beta=0$ ) for a standard dust composition and a covering factor  $f=0.8$ , in order to keep the number of free model parameters to a minimum. We have parameterized this class of models by the two parameters  $r_m/r_0$  and  $\tau_e$ . The former parameter is related mainly to the broadness of the IR bump, whereas the latter controls the near-to-

mid infrared slope of the SED along obscured lines of sight and the degree of its anisotropy.

Fig. 5 shows the colors predicted by the GD torus models as a function of  $r_m/r_0$  for different choices of the equatorial optical thickness  $\tau_e$ , in cases of face-on viewing angles. Fig. 6 show the analogous plots in cases of edge-on viewing angles. In Figs. 5 and 6 the two hatched regions mark the  $1-\sigma$  and  $2-\sigma$  error bands associated with the observed median. We show models with a standard silicate abundance and models with a typical depression of silicate grains in the innermost regions (i.e., for  $r \leq 50r_0$ ). The latter models are intended to give an indication of the effects of a silicate depression on the colors.

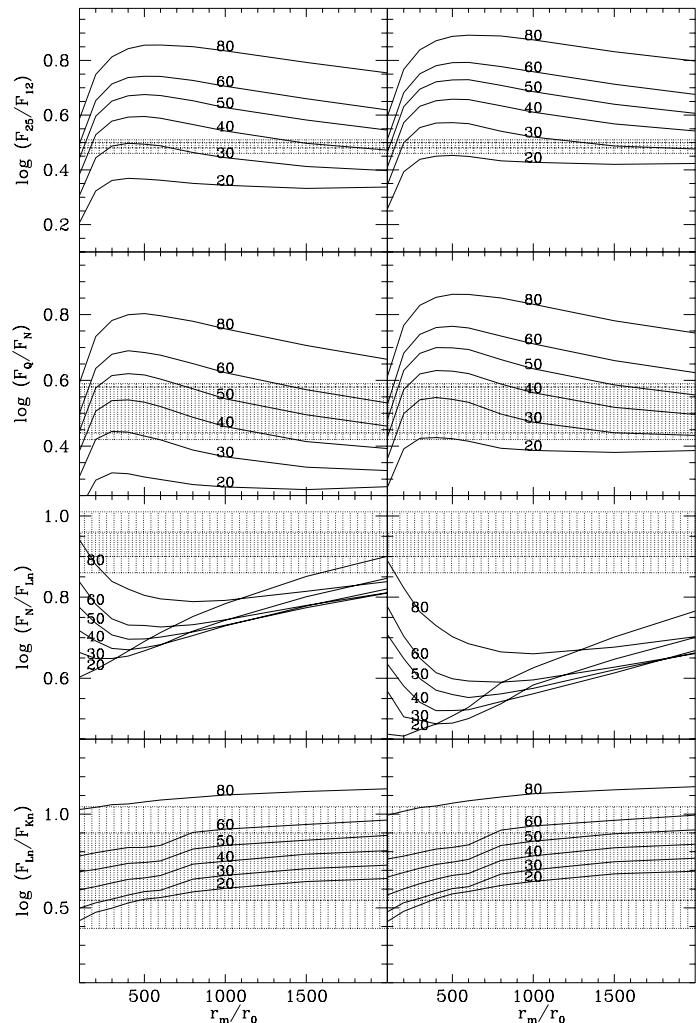


FIG. 6.— Same as in Fig. 5, but for an edge-on viewing angle.

Let us first look at the models with a standard silicate abundance. They always tend to give values for the color  $\log(F_{25}/F_{12})$  that are greater than for  $\log(F_Q/F_N)$  rather than vice-versa, as observed. The relatively high values of the latter quantity, namely the steepening of the SED as we go towards shorter wavelengths within the MIR spectral range, is not adequately reproduced by models.

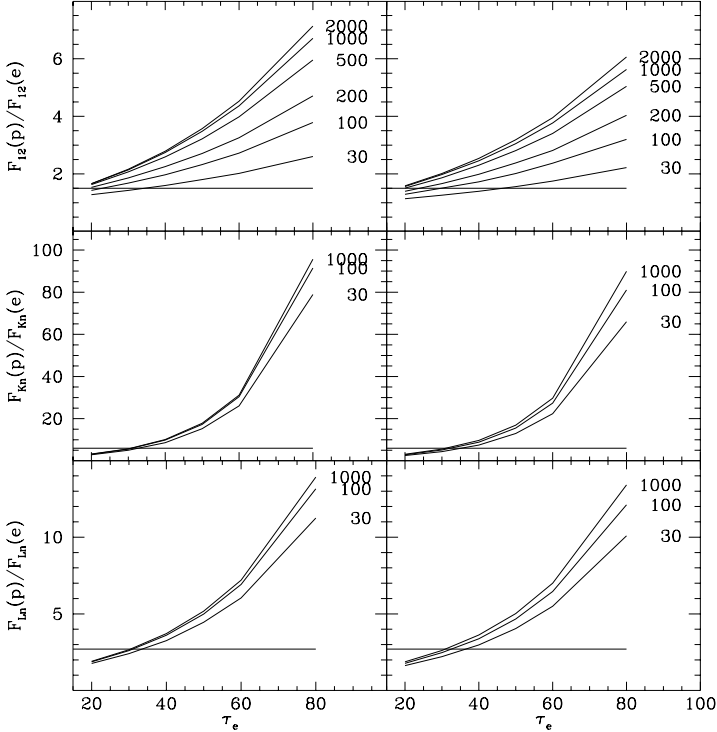


FIG. 7.— For some photometric bands the plots show the ratio between the fluxes received by a polar and an equatorial observer as a function of the equatorial optical thickness  $\tau_e$ , for different values of the outer-to-inner radius  $r_m/r_0$ . The horizontal lines denote the median values derived from the comparison of the IR luminosities of S1 and S2 nuclei. The left and right columns refer respectively to models with a standard silicate abundance and with a depression of silicates.

It is thus reasonable to be content with reproducing a typical mean MIR color  $\log(F_{25}/F_{12}) \sim \log(F_Q/F_N)$  of  $\sim 0.3-0.4$ . These values rule out compact tori (i.e. with  $r_m/r_0 \lesssim 100$ ). The color  $\log(F_N/F_{L_n})$  is easily accounted for by models characterized by relatively low values of  $r_m/r_0$  and  $\tau_e$  (e.g.,  $r_m/r_0 \sim 200$  and  $\tau_e \sim 20$ ) or by relatively high values of the two parameters (e.g.,  $r_m/r_0 \sim 700$  and  $\tau_e \sim 80$ ). In this case a decrease of  $r_m/r_0$  can be counterbalanced by an adequate decrease of  $\tau_e$ . A similar correlation between the two parameters holds for the color  $\log(F_{L_n}/F_{K_n})$ , which rejects models with low  $r_m/r_0$ -values (e.g., with  $r_m/r_0 \lesssim 300$  for  $\tau_e \sim 20$  or with  $r_m/r_0 \lesssim 1000$  for  $\tau_e \sim 80$ ). The color  $\log(F_{K_n}/F_{H_n})$  tends to reject tori of relatively small size and for very extended tori is not very sensitive to changes of  $r_m/r_0$  and  $\tau_e$ . The relatively low value of  $\log(F_{H_n}/F_{J_n})$  even more clearly favors very extended tori ( $r_m/r_0 \gtrsim 500$ ), within the usual  $\tau_e$ -interval.

The inclusion of silicate depression leaves the NIR SED almost unaffected, increases the MIR colors, and considerably reduces the color  $\log(F_N/F_{L_n})$ . These effects are similar for all viewing angles. For face-on viewing angles the MIR colors are now in better agreement with the obser-

vations. Now also  $\log(F_N/F_{L_n})$  agrees with the quantities  $\log(F_{L_n}/F_{K_n})$ ,  $\log(F_{K_n}/F_{H_n})$ ,  $\log(F_{H_n}/F_{J_n})$  in favoring very extended configurations. In summary, the IR colors better fit models of very extended tori ( $r_m/r_0 \gtrsim 500$ );  $\tau_e$  is not well constrained within the usual range ( $\tau_e \sim 20-80$ ). Notably, much larger and much lower values of  $\tau_e$  would give too steep and too flat MIR SEDs, respectively, for non-compact tori.

Let us discuss edge-on systems, disregarding the unreliable colors  $\log(F_{K_n}/F_{H_n})$  and  $\log(F_{H_n}/F_{J_n})$ . Tori of relatively small sizes ( $r_m/r_0 \sim 100$ ) can give realistic MIR colors and large enough values of  $\log(F_N/F_{L_n})$  for high values of  $\tau_e$ . Tori of intermediate sizes ( $r_m/r_0$ ) do not fit the color  $\log(F_N/F_{L_n})$  very well. Very extended tori can again well fit all colors. The inclusion of silicate depression does not change substantially the aforementioned considerations, although it tends to produce somewhat lower values of  $\log(F_N/F_{L_n})$  for very extended tori (for which, however, the assumption of uniform density distribution is likely to be less reasonable). But we have verified that the compatibility between the theoretical and observed values of  $\log(F_N/F_{L_n})$  for very extended tori critically depends on the adopted degree of silicate depression. A lower degree of depression (i.e., a depression within  $r \leq 15r_0$ ) gives great enough values of that color.

To sum up, for S2s the two fit parameters are poorly constrained; the data clearly rule out only very compact tori ( $r_m/r_0 \sim 10$ ), which would require unreasonably large values of  $\tau_e$ . Within the unified schemes of AGNs, we would prefer a solution involving very extended tori also for S2 galaxies. Although the theoretical colors do not unambiguously converge towards this solution for S2s, it is encouraging that this possibility is not seriously contradicted.

The comparison of the observed degree of anisotropy of the IR emission with the degree predicted by GD models provides a better constrain on  $\tau_e$  than that derived above. In Fig. 7 we show these predictions for some photometric bands by plotting the ratio between the fluxes received by a polar and by an equatorial observer as a function of  $\tau_e$ , for different values of  $r_m/r_0$ . The horizontal lines denote the median values (i.e. 1.5, 2.7, 6 for the 12  $\mu m$  -, L-, K-bands, respectively) that we derived in §3.2 by comparing the IR luminosities of S1 and S2 nuclei. Models with a standard silicate abundance (left column) and with a standard depression of silicate grains (right column) in the innermost regions (for  $r \leq 50r_0$ ) yield similar results for moderate values of  $\tau_e$ . These plots favor values of  $\tau_e$  ranging from  $\sim 20$  to  $\sim 40$  (i.e.  $10 \text{ mag} \lesssim A_V \lesssim 30 \text{ mag}$ ) for extended tori (with  $r_m/r_0 \gtrsim 100$ ).

## 5 SUMMARY AND CONCLUSIONS

We have undertaken a statistical analysis of the MIR and NIR fluxes of an extended sample of Seyfert galaxies, the widest Seyfert sample so far considered in the relevant literature. We have paid particular attention in selecting homogeneous data (when available) and nuclear data, i.e.

fluxes that are, as far as possible, free of stellar light contamination. This has enabled us to derive the NIR and MIR continuum emission properties of Seyfert nuclei with unprecedented accuracy. We can summarize our main results as follows.

The color distributions indicate that the typical SED of S2 nuclei is always steeper than that of S1 nuclei in the whole MIR and NIR spectral ranges. Hence S2s become typically fainter with respect to S1s as we go towards shorter IR wavelengths.

There is no sure evidence of bimodality in the color and luminosity distributions. This agrees with the absence of significant bimodality in the distributions of several emission properties of S1 and S2 galaxies, such as the ultraviolet, soft X-ray, hard X-ray emissions (Mulchaey et al., 1994) and radio core emission (Giuricin et al., 1996). A bimodality in some properties of S2s might be expected if there were two types of S2s, S2s with obscured BLR and without BLR, as was proposed by some authors (e. g., Hutchings & Neff, 1991; Moran et al., 1992).

The comparison of the IR luminosities of S1s and S2s, after they are made free of distance selection effects, reveals that S2s are somewhat brighter than S1s in the IRAS  $\lambda \sim 25 \mu\text{m}$  bands and in the IRAS FIR bands for the overall sample (though not for all subsamples). A direct comparison of the IR luminosities, normalized to those of the [OIII] emission line, confirms these results. This finding, which is unexpected within the framework of the unified model of Seyfert galaxies, can be explained in terms of observational selection effects favoring the inclusion of S2s with ongoing star formation in several current Seyfert samples, which are often dominated by optically-selected objects.

As we go to shorter wavelengths, S2s become increasingly fainter than S1s by an amount which is in fairly good, quantitative agreement with what we expect from the differences between their SEDs. Within the framework of torus models, this behavior is consistent with an increasing anisotropy of a torus emission towards shorter IR wavelengths. But the degree of anisotropy we derive is quite low (i.e. lower than what has frequently been claimed in the literature).

For a small sample of S2 galaxies having Compton-thin obscuring structures at hard X-ray energies, we discover significant correlations (previously unexplored) between the absorbing hydrogen columns derived from their hard X-ray spectra and some IR colors and luminosities. This indicates that the IR emitting torus is somehow related to the X-ray absorbing structure.

The typical shapes of the IR SEDs of S1s and S2s and the luminosity differences between the two types of objects (i.e. the degree of anisotropy of the IR radiation) are compared with the predictions of a wide series of torus models. Contrary to earlier claims, many models, in particular those involving compact or very thick configurations, are found to be basically inconsistent with the observational data.

We have specifically inspected the basic version of the torus models by Granato & Danese (1994), which was in-

tended to represent the simplest kind of tori envisaged by the AGN unification schemes. We have found that the major IR observational properties can be reasonably satisfied by flared disk configurations characterized by quite a large extension (a few hundreds pc) and moderate equatorial optical thickness (corresponding to a typical extinction of  $10 \text{ mag} \lesssim A_V \lesssim 30 \text{ mag}$ ), for both S1 and S2 galaxies.

For a standard dust over gas ratio, the aforementioned range of torus optical thickness, derived from fitting the IR properties of Seyfert nuclei, translates into lower values of  $N_H$  ( $N_H \sim 2 \cdot 10^{22} - 5 \cdot 10^{22} \text{ cm}^{-2}$ ) than the median value of  $N_H \sim 2.9 \cdot 10^{23} \text{ cm}^{-2}$  of a sample of S2 galaxies, which is still probably biased towards low values of  $N_H$ . This lends further support to the recent view that the matter responsible for the X-ray absorption is mostly dust-free and that the bulk of the X-ray absorption does not occur in the dusty torus, but at and just inside the dust sublimation radius (Granato et al., 1997).

Extended tori are consistent with the detection of dusty nuclear disks on scales of  $\sim 100$  pc in some *Hubble Space Telescope* observations (e.g., Jaffe et al., 1993) and with the detection of dense molecular nuclear disks on similar scales in some high-resolution radio observations (e.g., Tacconi et al., 1994; Kohno et al., 1996). Extended tori are also consistent with the presence of red (i.e. with  $V - R > 1.0$  mag) regions of hundreds of pc which coincide with the optical nuclei of many S2 objects; they can be interpreted as being due to reddening by dusty tori (Mulchaey et al., 1996b). It is known that there is a selection bias against finding AGNs (especially UV-excess AGNs and spectroscopically-selected AGNs) in highly inclined galaxies. This has led some authors to suggest that the obscuring material covers a part of the NLR (over  $\gtrsim 100$  pc) and is roughly coplanar with the host galaxy disk (McLeod & Rieke, 1995; Maiolino & Rieke, 1995).

Extended configurations are also in better agreement than compact tori (with a radial size of  $\lesssim 10$  pc) with the high-resolution NIR and MIR observations of NGC 1068, which showed an emission extended over  $\sim 1''$  scale (e.g., McCarthy et al., 1982; Chelli et al., 1987; Tresch-Fienberg et al., 1987; Braatz et al., 1993; Cameron et al., 1993). If this emission were due to torus radiation reflected by electron scattering and to NLR dust (Pier & Krolik, 1993), there would probably be too large reddening in the NLR (Cameron et al., 1993). The analysis of NIR polarized images of the nuclear region of this galaxy points to a torus with a size of  $\sim 200$  pc (Young et al., 1996b). An extended ( $\sim 2''$ ) bar-like NIR emission, which might hint at an extended dusty torus viewed approximately edge-on, has been recently detected in Mk 348 (Simpson et al., 1996).

Tori with moderate optical depths are consistent with the detection of broad components of NIR lines in several narrow-line AGNs (as discussed by Granato et al., 1997). In most cases of detections of broad lines in a seeming narrow-line object, the broad lines are reddened more than the narrow lines, locating the bulk of the dust re-

sponsible for absorbing the broad-line emission between the BLR and the NLR (e.g., Hill, Goodrich & DePoy, 1996). Narrow-line galaxies which do not show broad lines in total or polarized flux could have obscured regions of scattered radiation or lines which are thermally very broadened and hence hardly observable (see, e.g., Young et al., 1996a). Moderate optical depths are also consistent with the typical extinctions ( $A_V \lesssim 30$  mag) inferred from the strengths of the  $10 \mu\text{m}$  silicate absorption features observed in several S2 galaxies (e.g., Aitken & Roche, 1985; Roche et al., 1991).

Alleviating some earlier worries, we can conclude that the general unified scheme of AGNs is basically compatible with the IR observational data. Notably, this scheme can not hold in a strict sense, since the broadness of the color distributions suggests a large spread in the properties of obscuring tori, especially for S2s. Other arguments against the strict version of the unified scheme can be found in Antonucci's (1993) review.

There is no indication in our sample that the optical depth of tori decreases with AGN luminosity, as is advocated by the simplest modification of the strict unified scheme (e.g., Lawrence, 1991). By the way, the SEDs of some hyperluminous high-redshift IR galaxies have been recently reproduced in terms of a luminous AGN surrounded by an extended torus with a larger equatorial optical depth ( $60 \text{ mag} \lesssim A_V \lesssim 300 \text{ mag}$ ) than those of classical Seyfert galaxies (Granato, Danese & Franceschini, 1996). The ISO satellite observations are expected to sub-

stantially improve our knowledge of the IR properties of high-luminosity AGNs.

Nevertheless, our detailed comparison with the observational data raises several problems. Also the most successful torus models, i.e. extended and moderately thick flared disks, fail to reproduce accurately several observational details. Even with the present quality and quantity of observations there is a need for more sophisticated versions of torus models having more free parameters to fit the data (e.g., different matter distributions and geometries), though not so many as to preclude physical understanding. Remarkably, especially in the case of extended configurations, the possible clumpy nature of the actual dust distribution weakens the validity of current torus models, which are based on a continuous distribution of matter.

The authors are grateful to L. Danese for enlightening discussions on torus models and to M. Mezzetti for comments on the statistical analysis.

The authors thank E. D. Feigelson for having kindly provided the ASURV software package.

This research has made use of the NASA/IPAC Extragalactic Database (NED), which is operated by the Jet Propulsion Laboratory, Caltech, under contract with the National Aeronautics and Space Administration.

This work has been partially supported by the Italian Ministry of University, Scientific, and Technological Research (MURST) and by the Italian Space Agency (ASI).

## REFERENCES

- Aitken, D. K. & Roche, P. F., 1985, *MNRAS*, 213, 777.  
 Alonso-Herrero, A., Ward, M. J. & Kotilainen, J. K., 1996, *MNRAS*, 278, 902.  
 Antonucci, R. R. J., *ARA&A*, 31, 473.  
 Barcons, X., Franceschini, A., De Zotti, G., Danese, L. & Miyaji, T., 1995, *ApJ*, 455, 480.  
 Barvainis, R., 1987, *ApJ*, 320, 537.  
 Barvainis, R., 1990, *ApJ*, 353, 419.  
 Barvainis, R., 1992, in "Testing the AGN paradigm", S. Holt, S. Neff & M. Urry eds. (New York: AIP), 129.  
 Beichman, C. A., Neugebauer, G., Habing, H. J., Clegg, P. E. & Chester, T. J., 1988, *IRAS Catalogs and Atlases: Explanatory Supplement* (Washington, DC: GPO).  
 Bessell, M. S. & Brett, J. M., 1988, *PASP*, 100, 1134.  
 Binette, L., Fosbury, R. A. & Parker, D., 1993, *PASP*, 105, 1150.  
 Blanco, P. R., Ward, M. J. & Wright, C. S., 1990, *MNRAS*, 242, 4P.  
 Boisson, C. & Durret, F., 1986, *A&A*, 168, 32.  
 Bothun, G. D., Halpern, J. P., Lonsdale, C. J., Impey, C., Schmitz, M., 1989, *ApJS*, 70, 271.  
 Braatz, J. A., Wilson, A. S., Gezari, D. Y., Varosi, F. & Beichman, C. A., *ApJ*, 409, L5.  
 Cameron, M. et al., 1993, *ApJ*, 419, 136.  
 Campins, H., Rieke, G. H. & Lebofsky, M. J., 1985, *AJ*, 90, 896.  
 Carico, D. P. et al., 1988, *AJ*, 95, 356.  
 Chelli, A., Perrier, C., Cruz-Gonzales, I. & Carrasco, L., 1987, *A&A*, 177, 52.  
 Dahari, O. & De Robertis, 1988, *ApJS*, 67, 249.  
 Danese, L., Zitelli, V., Granato, G., Wade, R., De Zotti, G. & Mandolesi, N., 1992, *ApJ*, 399, 38.  
 de Grijp, M. H. K., Keel, W. C., Miley, G. K., Goudfrooij, P. & Lub, J., *A&AS*, 96, 389.  
 Edelson, R. & Malkan, M. A., 1987, *ApJ*, 323, 516.  
 Edelson, R., Malkan, M. A. & Rieke, G. H., 1987, *ApJ*, 321, 233.  
 Efstathiou, A., Hough, J. H. & Young, S., 1996, *MNRAS*, 277, 1134.  
 Efstathiou, A. & Rowan-Robinson, M., 1995, *MNRAS*, 273, 649 (ER).  
 Elvis, M., Willner, S. P., Fabbiano, G. et al., 1984, *ApJ*, 280, 574.  
 Evans, I. N., Koratkar, A. P., Storchi-Bergmann, T. et al., 1996, *ApJS*, 105, 93.  
 Feigelson, E. D. & Nelson, P. I., 1985, *ApJ*, 293, 192.  
 Gezari, D. Y., Schmitz, M., Pitts, P. S. & Mead, J. M., 1993, "Catalog of Infrared Observations", NASA Reference Publication No. 1294.  
 Giuricin, G., Fadda, D. & Mezzetti, *ApJ*, 468, 475.  
 Giuricin, G., Mardirossian, F. & Mezzetti, M., 1995, *ApJ*, 446, 550.  
 Giuricin, G., Tamburini, L., Mardirossian, F., Mezzetti, M. & Monaco, P., 1994, *ApJ*, 427, 202.  
 Glass, I. S., 1992, *MNRAS*, 256, 23 p.  
 Glass, I. S. & Moorwood, A. F. M., 1985, *MNRAS*, 214, 429.  
 Golombek, D., Miley, G. K. & Neugebauer, G., 1988, *AJ*, 95, 26.  
 Goodrich, R. W., Veilleux, S. & Hill, G. J., 1994, *ApJ*, 422, 521.  
 Granato, G. & Danese, L., 1994, *MNRAS*, 268, 235 (GD).  
 Granato, G., Danese, L. & Franceschini, A., 1996, *ApJ*, 460, L11.  
 Granato, G., Danese, L. & Franceschini, A., 1997, *ApJ*, in press.  
 Heckman, T. M., 1995, *ApJ*, 446, 101.  
 Heisler, C. A., De Robertis, M. M. & Nadeau, D., 1996, *MNRAS*, 280, 579.  
 Helou, G., Khan, I. R., Malek, L. & Boehmer, L., 1988, *ApJS*, 68, 151.  
 Hes, R., Barthel, P. D. & Fosbury, R. A., 1993, *Nature*, 362, 326.  
 Hill, G. J., Becklin, E. E. & Wynn-Williams, C. G., 1988, *ApJ*, 330, 737.  
 Hill, G. J., Goodrich, R. W. & DePoy, D. L., 1996, *ApJ*, 462, 163.  
 Hoel, P. G., 1971, *Introduction to Mathematical Statistics* (4th ed.: New York, Wiley).  
 Hutchings, J. B. & Neff, S. G., 1991, *AJ*, 101, 434.

- Isobe, T., Feigelson, E. D. & Nelson, P. J., 1986, *ApJ*, 306, 490.
- Iwasawa, K., 1996, Ph.D. thesis, ISAS.
- Jackson, N. & Browne, I. W., 1990, *Nature*, 343, 43.
- Jaffe, W., Ford, H. C., Ferrarese, L., Van den Bosch, F. & O'Connell, R. W., 1993, *Nature*, 364, 213.
- Laing, R. A., Jenkins, C. R., Wall, J. V. & Unger, S. W., 1994, in *ASP Conf. Ser. 54, The First Stromlo Symposium: The Physics of Active Galaxies*, eds. G.V. Bicknell, M. A. Dopita & P. J. Quinn (San Francisco: ASP), 175.
- Lawrence, A., 1991, *MNRAS*, 252, 586.
- Keel, W. C., de Grijp, M. H. K., Miley, G. K. & Zheng, W., 1994, *A&A*, 283, 791.
- Kendall, M. & Stuart, A., 1977, *The Advanced Theory of Statistics* (London: Griffin).
- Knapp, G. R., Bies, W. E. & van Gorkom, J. H., 1990, *AJ*, 99, 476.
- Knapp, G. R., Guhathakurta, P., Kim, D.-W. & Jura, M., 1989, *ApJS*, 70, 329.
- Kohno, K., Kawabe, R., Tosaki, T. & Okumura, S. K., 1996, *ApJ*, 461, L29.
- Kotilainen, J. K. & Prieto, M. A., 1995, *A&A*, 295, 646.
- Kotilainen, J. K., Ward, M. J., Boisson, C., DePoy, D. L., Bryant, L. R., Smith, M. G., 1992a, *MNRAS*, 256, 125.
- Kotilainen, J. K., Ward, M. J., Boisson, C., DePoy, D. L., Bryant, L. R., Smith, M. G., 1992b, *MNRAS*, 256, 149.
- Laor, A. & Draine, B. T., 1993, *ApJ*, 402, 441.
- La Valley, M. Isobe, T. & Feigelson, E. D., 1992, *BAAS*, 24, 839.
- Lawrence, A. et al., 1985, *ApJ*, 291, 117.
- Loska, Z., Szczerba, R. & Czerny, B., 1993, *MNRAS*, 261, 63.
- Maiolino, R. & Rieke, G. H., 1995, *ApJ*, 454, 95.
- Maiolino, R., Ruiz, M., Rieke, G. H. & Keller, L. D., 1995, *ApJ*, 446, 561.
- Matt, G., Fiore, F., Perola, G. C. et al., 1996, *MNRAS*, 281, L69.
- Mazzarella, J. M., Bothun, G. D. & Boroson, T. A., 1991, *AJ*, 101, 2034.
- McAlary, C. W., McLaren, R. A. & Crabtree, D. R., 1979, *ApJ*, 234, 471.
- McAlary, C. W., McLaren, R. A., McGonegal, R. J., Maza, J., 1983, *ApJS*, 52, 341.
- McAlary, C. W. & Rieke, G. H., 1988, *ApJ*, 333, 1.
- McCarthy, D. W., Low, F. J., Kleinmann, S. G. & Gillet, F. C., 1982, *ApJ*, 257, L7.
- McLeod, K. K. & Rieke, G. H., 1995, *ApJ*, 441, 96.
- Miles, J. W., Houck, J. R., & Hayward, T. L., 1994, *ApJ*, 425, L37.
- Moran, E. C., Halpern, J. P., Bothun, G. D. & Becker, R. H., 1992, *AJ*, 104, 990.
- Moshir, M. et al., 1992, *Explanatory Supplement to the IRAS Faint Source Survey, Ver. 2* (Pasadena: JPL).
- Mulchaey, J. S., Koratkar, A., Ward, J. et al., 1994, *ApJ*, 436, 586.
- Mulchaey, J. S., Wilson, A. S. & Tsvetanov, Z., 1996a, *ApJS*, 102, 309.
- Mulchaey, J. S., Wilson, A. S. & Tsvetanov, Z., 1996b, *ApJ*, 467, 197.
- Nandra, K. & Pounds, K. A., 1994, *MNRAS*, 268, 405.
- Nelson, C. H. & Whittle, M., 1995, *ApJS*, 99, 67.
- Neugebauer, G., Green, R. F., Matthews, K. et al., 1987, *ApJS*, 63, 615.
- Neugebauer, G., Soifer, B. T., Matthews, K. & Elias, J. H., 1989, *AJ*, 97, 957.
- Osterbrock, D. E. & Martel, A., 1993, *ApJ*, 414, 552.
- Phinney, E. S., 1989, in *Theory of Accretion Disks*, ed. J. S. Meyer (Dordrecht: Kluwer), 457.
- Pier, E. A. & Krolik, J. H., 1992, *ApJ*, 401, 99 (PK).
- Pier, E. A. & Krolik, J. H., 1993, *ApJ*, 418, 673.
- Pogge, R. W., 1989, *ApJ*, 345, 730.
- Rice, W., Lonsdale, C. J., Soifer, B. T. et al., 1988, *ApJS*, 68, 151.
- Rieke, G. H., 1978, *ApJ*, 226, 550.
- Roche, P. F., Aitken, D. A., Smith, C. H. & Ward, M., 1991, *MNRAS*, 248, 606.
- Rudy, R. J., Levan, P. D. & Rodríguez-Espinosa, J. M., 1982, *AJ*, 87, 599.
- Rudy, R. J. & Rodríguez-Espinosa, J. M., 1985, *ApJ*, 298, 614.
- Ruiz, M., Rieke, G. H. & Schmidt, G. D., 1994, *ApJ*, 423, 608.
- Rush, B., Malkan, M. A. & Spinoglio, L., 1993, *ApJS*, 89, 1.
- Salzer, J. J. & MacAlpine, G. M., 1988, *AJ*, 96, 1192.
- Sanders, D.B., Egami, E., Mirabel, I. F. & Soifer, B. T., 1995, *AJ*, 110, 1993.
- Sanders, D. B., Phinney, E. S., Neugebauer, G., Soifer, B. T. & Matthews, K., 1989, *ApJ*, 347, 29.
- Shapiro, S. S. & Wilk, M. B., 1965, *Biometrika*, 52, 591.
- Simpson, C., Mulchaey, J. S., Wilson, A. S., Ward, M. J. & Alonso-Herrero, A., 1996, *ApJ*, 457, L19.
- Smith, D. A. & Done, C., 1996, *MNRAS*, 280, 355.
- Soifer, B. T., Boehmer, L., Neugebauer, G. & Sanders, D. B., 1989, *AJ*, 98, 766.
- Spinoglio, L. & Malkan, M. A., 1989, *ApJ*, 342, 83.
- Spinoglio, L., Malkan, M. A., Rush, B., Carrasco, L. & Recillas-Cruz, E., 1995, *ApJ*, 453, 616.
- Stein, W. A. & Weedman, D.W., 1976, *ApJ*, 205, 44.
- Tacconi, L. J., Genzel, R., Blietz, M. et al., 1994, *ApJ*, 426, L77.
- Telesco, C. M., 1988, *ARA&A*, 26, 343.
- Telesco, C. M., & Decher, R., 1988, *ApJ*, 334, 573.
- Telesco, C. M., Dressel, L. L., & Wolstencroft, R. D., 1993, *ApJ*, 414, 120.
- Tresch-Fienberg, R. et al., 1987, *ApJ*, 312, 542.
- Tully, R. B., 1988, *Nearby Galaxies Catalog* (Cambridge: Cambridge Univ. Press).
- Vader, P. J., Frogel, J. A., Terndrup, D. M. & Heisler, C. A., 1993, *AJ*, 106, 1743.
- Véron-Cetty, M. P. & Véron, P., 1991, *A Catalogue of Quasars and Active Nuclei*, 7th ed. (ESO Sci. Rep. No. 17).
- Ward, M. et al., 1987, *ApJ*, 315, 74.
- Warwick, R. S., Sembay, S., Yaqoob, T. et al., 1993, *MNRAS*, 265, 412.
- Whittle, M., 1992, *ApJS*, 79, 49.
- Willner, S. P. et al., 1984, *PASP*, 96, 143.
- Wilson, A. S., 1992, in "Physics of Active Galactic Nuclei", eds. W. J. Duschl & S. J. Wagner (Springer Verlag: Heidelberg), 307.
- Wilson, A. S., 1996, *Vistas in Astronomy*, 40, 63.
- Wilson, W. J., Schwartz, P. R., Neugebauer, G., Harvey, P. M. & Becklin, E. E., 1972, *ApJ*, 177, 523.
- Wynn-Williams, C. G. & Becklin, E. E., 1993, *ApJ*, 412, 535.
- Young, S., Hough, J. H., Efstathiou, A., Wills, B. J., Bailey, J. A., Ward, M. J. & Axon, D. J., 1996a, *MNRAS*, 281, 1206.
- Young, S., Packham, C., Hough, J. H. & Efstathiou, A., 1996b, *MNRAS*, 283, L1.
- Zhou, S., Wynn-Williams, C. G. & Sanders, D. B., 1993, *ApJ*, 409, 149.
- Zitelli, V., Granato, G., Mandolesi, N., Wade, R. & Danese, L., 1993, *ApJS*, 84, 185.